Cell Reports

Article

Vitamin B5 rewires Th17 cell metabolism via impeding PKM2 nuclear translocation

Graphical abstract

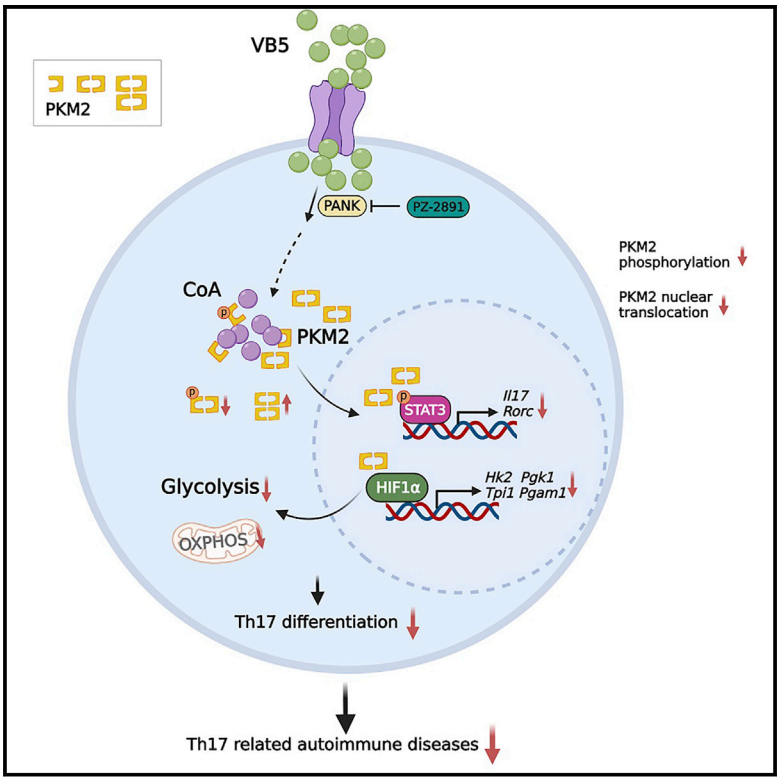

Highlights

- Vitamin B5 rewires Th17 cell metabolism and restrains Th17 cell differentiation
- Vitamin B5 ameliorates Th17-associated autoimmune disorders EAE and colitis
- Coenzyme A catabolized from vitamin B5 binds to PKM2 to impede its nuclear translocation
- Vitamin B5 is much lower in serum of ulcerative colitis and multiple sclerosis patients

Authors

Chen Chen, Weiqiao Zhang, Tingyue Zhou, ..., Wei Jiang, Wen Pan, Shu Zhu

Correspondence

ustcjw@ustc.edu.cn (W.J.), zhushu@ustc.edu.cn (S.Z.)

In brief

In this study, Chen et al. report that diet-derived vitamin B5 restrains Th17 cell differentiation and Th17-associated autoimmune diseases by impeding PKM2 nuclear translocation, thus inhibiting glycolysis and STAT3 phosphorylation. This finding shows a role of VB5 in Th17 cell metabolic rewiring and Th17-associated disease intervention.

Chen et al., 2022, Cell Reports *41*, 111741
November 29, 2022
https://doi.org/10.1016/j.celrep.2022.111741

CellPress

Cell Reports

CellPress
OPEN ACCESS

Article

Vitamin B5 rewires Th17 cell metabolism via impeding PKM2 nuclear translocation

Chen Chen,[1,2,8] Weiqiao Zhang,[1,2,8] Tingyue Zhou,[1,2] Qiuyuan Liu,[3] Chao Han,[4] Zonghui Huang,[2] Si Chen,[1] Qiao Mei,[3] Cunjin Zhang,[5] Kaiguang Zhang,[1] Hongdi Ma,[1,2] Rongbin Zhou,[2,7] Wei Jiang,[2,*] Wen Pan,[1,2] and Shu Zhu[1,2,6,7,9,*]

[1]Department of Digestive Disease, The First Affiliated Hospital of USTC, Division of Life Sciences and Medicine, University of Science and Technology of China, Hefei 230001, China

[2]Institute of Immunology, The CAS Key Laboratory of Innate Immunity and Chronic Disease, Division of Life Sciences and Medicine, University of Science and Technology of China, Hefei 230001, China

[3]Department of Gastroenterology, The First Affiliated Hospital of Anhui Medical University, Hefei 230022, China

[4]Department of Neurology, The First Affiliated Hospital of USTC, Division of Life Sciences and Medicine, University of Science and Technology of China, Hefei 230001, China

[5]Department of Neurology, Drum Tower Hospital, Medical School and the State Key Laboratory of Pharmaceutical Biotechnology, Institute of Brain Science, Nanjing University, Nanjing 210008, China

[6]School of Data Science, University of Science and Technology of China, Hefei 230026, China

[7]Institute of Health and Medicine, Hefei Comprehensive National Science Center, Hefei, China

[8]These authors contributed equally

[9]Lead contact

*Correspondence: ustcjw@ustc.edu.cn (W.J.), zhushu@ustc.edu.cn (S.Z.)

https://doi.org/10.1016/j.celrep.2022.111741

SUMMARY

Metabolic rewiring is essential for Th17 cells' functional identity to sense and interpret environmental cues. However, the environmental metabolic checkpoints with specific regulation of Th17 cells, manifesting potential therapeutic opportunities to autoimmune diseases, remain largely unknown. Here, by screening more than one hundred compounds derived from intestinal microbes or diet, we found that vitamin B5 (VB5) restrains Th17 cell differentiation as well as related autoimmune diseases such as experimental autoimmune encephalomyelitis and colitis. Mechanistically, VB5 is catabolized into coenzyme A (CoA) in a pantothenate kinase (PANK)-dependent manner, and in turn, CoA binds to pyruvate kinase isoform 2 (PKM2) to impede its phosphorylation and nuclear translocation, thus inhibiting glycolysis and STAT3 phosphorylation. In humans, reduced serum VB5 levels are found in both IBD and MS patients. Collectively, our study demonstrates a role of VB5 in Th17 cell metabolic reprograming, thus providing a potential therapeutic intervention for Th17 cell-associated autoimmune diseases.

INTRODUCTION

Th17 cells are a $CD4^+$ T helper cell subset, characterized by production of cytokine IL-17A, IL-17F, and granulocyte-macrophage colony-stimulating factor (GM-CSF).[1–3] T cell receptor (TCR) signaling combined with cytokine milieus IL-6, TGF-β1, and IL-23 to direct Th17 cell differentiation by inducing phosphorylation of STAT3 and transcription of RAR-related orphan receptor gamma (RORγt),[4,5] the lineage-specific transcription factor of Th17 cells. Th17 cells are abundant in intestinal mucosal barrier to maintain epithelial integrity, and to protect hosts from extracellular bacterial and fungal infections in homeostasis.[6–9] However, uncontrolled Th17 cell responses leads to autoimmune inflammation, including multiple sclerosis (MS), inflammatory bowel disease (IBD), psoriasis, and ankylosing spondylitis (AS),[7,10,11] many of which lack effective therapies. Understanding the mechanisms that govern the Th17 cell differentiation and pathogenicity may provide potential therapeutic intervention for treating multiple Th17 cell-associated autoimmune diseases.

Emerging literatures suggest that interplay between metabolic pathways and cytokines potentiates T cell differentiation and functions in tissue inflammation and autoimmune diseases. Studies have demonstrated a shift from oxidative phosphorylation to aerobic glycolysis during naive $CD4^+$ T cell differentiation toward Th17 cells.[12–14] Also, there are reports showing that commensal bacteria (e.g., SFB)-induced homeostatic Th17 cells rely mainly on oxidative phosphorylation, whereas pathogen (e.g., *Citrobacter rodentium*) elicited pro-inflammatory Th17 cells are highly glycolytic.[15] These metabolic pathways, together with mammalian target of rapamycin (mTOR)-mediated signals, are essential for Th17 cell differentiation and pro-inflammatory function.[16–19] Pharmacological inhibition of mitochondrial oxidative phosphorylation under Th17 cell differentiation conditions *in vitro* resulted in expression of regulatory T cell signature genes, rather than Th17 cell-associated gene expression.[20] Genetic deficiency of molecules involved in glycolysis and mTOR signaling, such as *Hif1α* (glycolysis),[16,17] *Rheb*, and *Rictor* (mTOR)[15,18,19] significantly impaired Th17 cell differentiation and pro-inflammatory function.

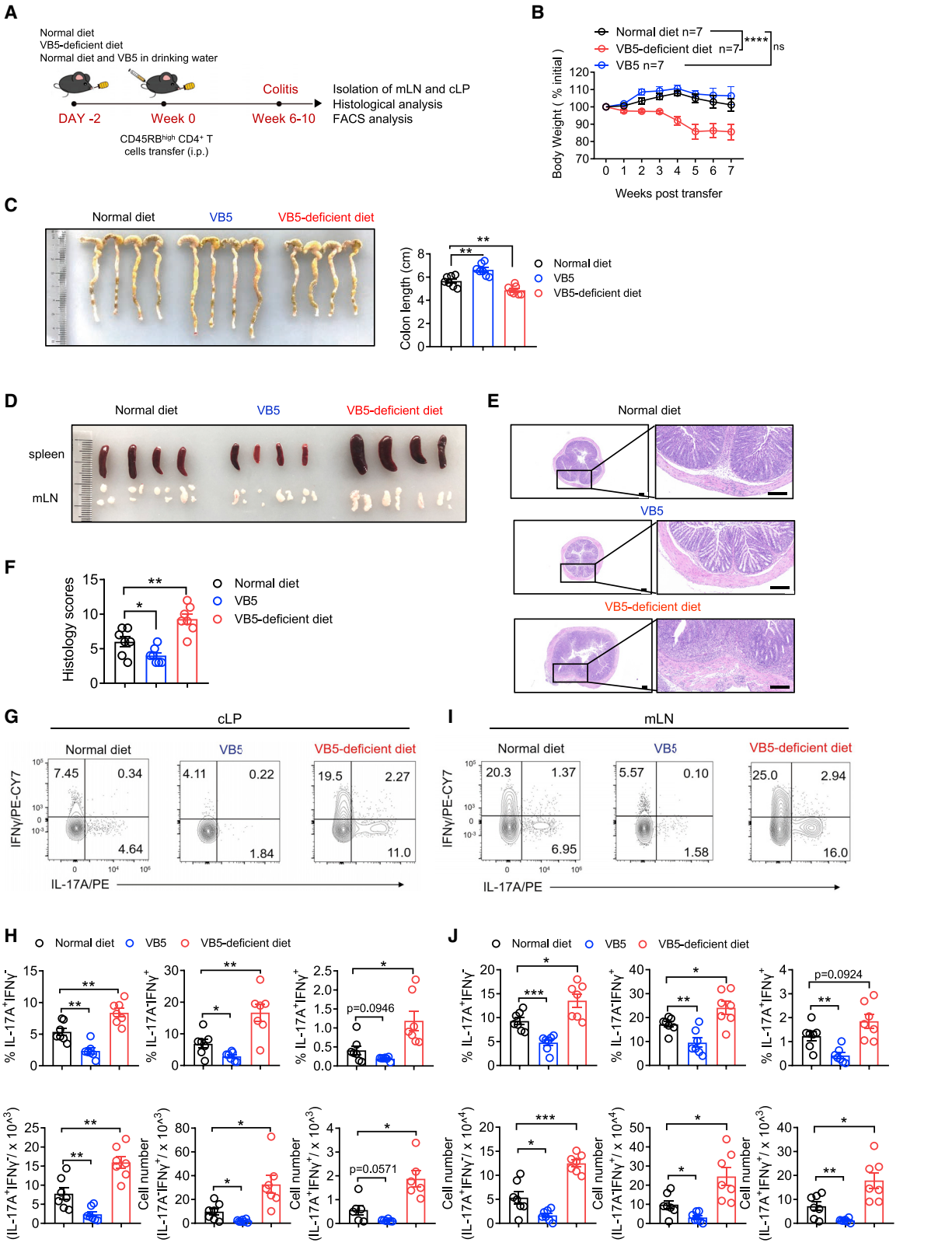

(legend on next page)

Pyruvate kinase isoform 2 (PKM2) is a glycolytic enzyme that catalyzes the conversion of phosphoenolpyruvate (PEP) to pyruvate and has been shown as an important determinant of metabolic reprogramming in macrophage.[21] The dimeric and monomeric forms of PKM2 are enzymatically less active than the tetrameric isoform and are able to translocate into the nucleus, wherein they can interact with HIF1α to regulate glycolytic gene expression.[22] In contrast, tetrameric PKM2 is cytosol localized and functions to catalyze the last step of glycolysis: converting phosphoenolpyruvate to pyruvate, redundant with PKM1 activity.[23] During Th17 cell differentiation, inhibition of enzymatic activity of PKM2 by shikonin is shown to inhibit both glycolysis and pro-inflammatory cytokine production.[24] It has also been shown that impeding PKM2 nuclear translocation using a compound TEPP-46 reduced inflammatory cytokine expression in Th17 cells and reduced HIF1α- and mTORC1-targeted gene expression.[25] Nuclear PKM2 is shown to interact with STAT3 and to enhance STAT3 phosphorylation under Th17-skewing conditions.[23] These studies demonstrated PKM2 is important for Th17 cell differentiation and function. Better understanding of the modulation of the metabolic checkpoints such as PKM2 may potentially lead to a therapeutic strategy for Th17-mediated autoimmune diseases.

Environmental factors such as microbes (e.g., SFB, *C. rodentium*, *Candida albicans*)[26–28] or dietary components (high salt, high glucose)[29–31] are reported to regulate Th17 differentiation through different pathways. However, environmental metabolic checkpoints with specific regulation of Th17 cells, manifesting potential therapeutic opportunities to Th17 cell-mediated autoimmune diseases, remain unknown. Here, by screening more than one hundred compounds derived from intestinal microbes or diet, we found that diet-derived vitamin B5 (VB5) protects against autoimmune diseases in experimental colitis and experimental autoimmune encephalomyelitis (EAE) models by restraining Th17 cell differentiation. In contrast, VB5 deficiency render mice prone to experimental colitis and EAE. We further elucidated that VB5 restrains Th17 cell differentiation by impeding PKM2 nuclear translocation, thus inhibiting glycolysis and STAT3 phosphorylation. Moreover, IBD and MS patients have reduced serum VB5 levels compared with healthy controls, and VB5 also inhibits human Th17 cell differentiation *in vitro*. Thus, our study has revealed an unrecognized role of VB5 in restraining Th17 cell differentiation and protecting against autoimmune diseases.

RESULTS

Vitamin B5 suppresses experimental colitis

To investigate whether intestinal environmental cues can exert protective effect(s) on autoimmune inflammation mediated by inflammatory Th17 cells, we conducted an *in vitro* screen of more than one hundred intestinal compounds (including both diet- and bacteria-derived compounds) by using an IL-17A-IRES-GFP reporter system showing the differentiation status of Th17 cells.[32] On the basis of monitoring the frequency of IL-17A-producing cells, this screen identified, for example, that the intestinal bacteria-derived short chain fatty acid compound butyrate dramatically restrains Th17 cell differentiation, a finding consistent with many previous reports[33,34] (Figures S1A–S1C). Notably, VB5 exerted the strongest suppressive effect on Th17 cell differentiation among all the metabolites we screened (Figure S1C), which is not reported before.

We next used a naive CD4$^+$ T cell-transfer colitis model to evaluate if VB5 affects Th17-associated autoimmune disease *in vivo* (Figure 1A). Specifically, CD25$^-$CD45RB^{hi} naive CD4$^+$ T cells were transferred into lymphopenic *Rag1*$^{-/-}$ mice to induce colitis. Two days before transfer of the CD25$^-$CD45RB^{hi} naive CD4$^+$ T cells, recipient mice were provided with normal diet, VB5-deficient diet, or normal diet with VB5 in drinking water (Figures 1A and S2A). Compared with the normal diet control animals, mice fed with VB5-deficient diet showed more body weight loss (Figure 1B) and displayed more severe colitis, reflecting by shortened colon lengths (Figure 1C) and swollen spleen and mesenteric lymph node (mLN) (Figure 1D). Consistently, histopathological analysis with H&E staining showed that VB5-deficient diet-fed mice had higher immune cell infiltration, thicker colonic wall, and much more disrupted crypt structures than normal diet-fed mice (Figures 1E and 1F). We further analyzed CD4$^+$ effector T cells in the colon and mLN. We observed that VB5-deficient diet-fed mice had significantly increased frequency and cell number of IL-17A$^+$ cells in the lamina propria and mLN (Figures 1G–1J and S2B), compared with normal diet-fed mice. IL-17A$^-$ IFNγ^+ CD4$^+$ T cells were also increased in VB5-deficient diet-fed mice compared with normal diet-fed mice (Figures 1G–1J). qPCR analysis of colon also showed increased *Il17a*, *Ifng*, *Csf2*, *Il22*, and *Il23r* mRNA expression in VB5-deficient diet treatment, while the expression of immune regulatory genes *Il10* and *Foxp3* was downregulated (Figure S2C).

Figure 1. VB5-deficient diet-treated mice are susceptible to colitis

(A) Schematic of the experimental design. Lymphopenic *Rag1*$^{-/-}$ mice transferred with CD45RB^{hi} naive CD4$^+$ T cells were fed with normal diet/normal water, VB5-deficient diet/normal water, or normal diet/VB5 water two days before T cell transfer, and mice were monitored for colitis development.

(B) Monitoring of body weight after the transfer of CD45RB^{hi} naive CD4$^+$ T cells (n = 7).

(C) Colon length in indicated groups of mice (n = 7).

(D) Histological images of the spleens and mesenteric lymph nodes (mLN) of the indicated mice.

(E) Representative H&E staining of colon sections from the indicated mice. Scale bars, 200 μm.

(F) Quantification of colon pathology of the indicated mice (n = 7).

(G–J) Representative fluorescence-activated cell sorting (FACS) plots (G and I) and quantification (H and J) showing the percentage and absolute numbers of IL-17A$^+$IFNγ^-, IL-17A$^+$IFNγ^+, IL-17A$^-$IFNγ^+ CD4$^+$ T cells in the colonic lamina propria (cLP) (G and H) and mLN (I and J) from indicated mice (n = 7).

Data in (A)–(J) are representative of three independent experiments. All data are mean ± SEM and were analyzed using two-way ANOVA with Tukey's multiple-comparisons test (B) and the two-tailed, unpaired Student's t test (C, F, H, and J). *p < 0.05, **p < 0.01, ***p < 0.001, and ****p < 0.0001. See also Figures S1 and S2.

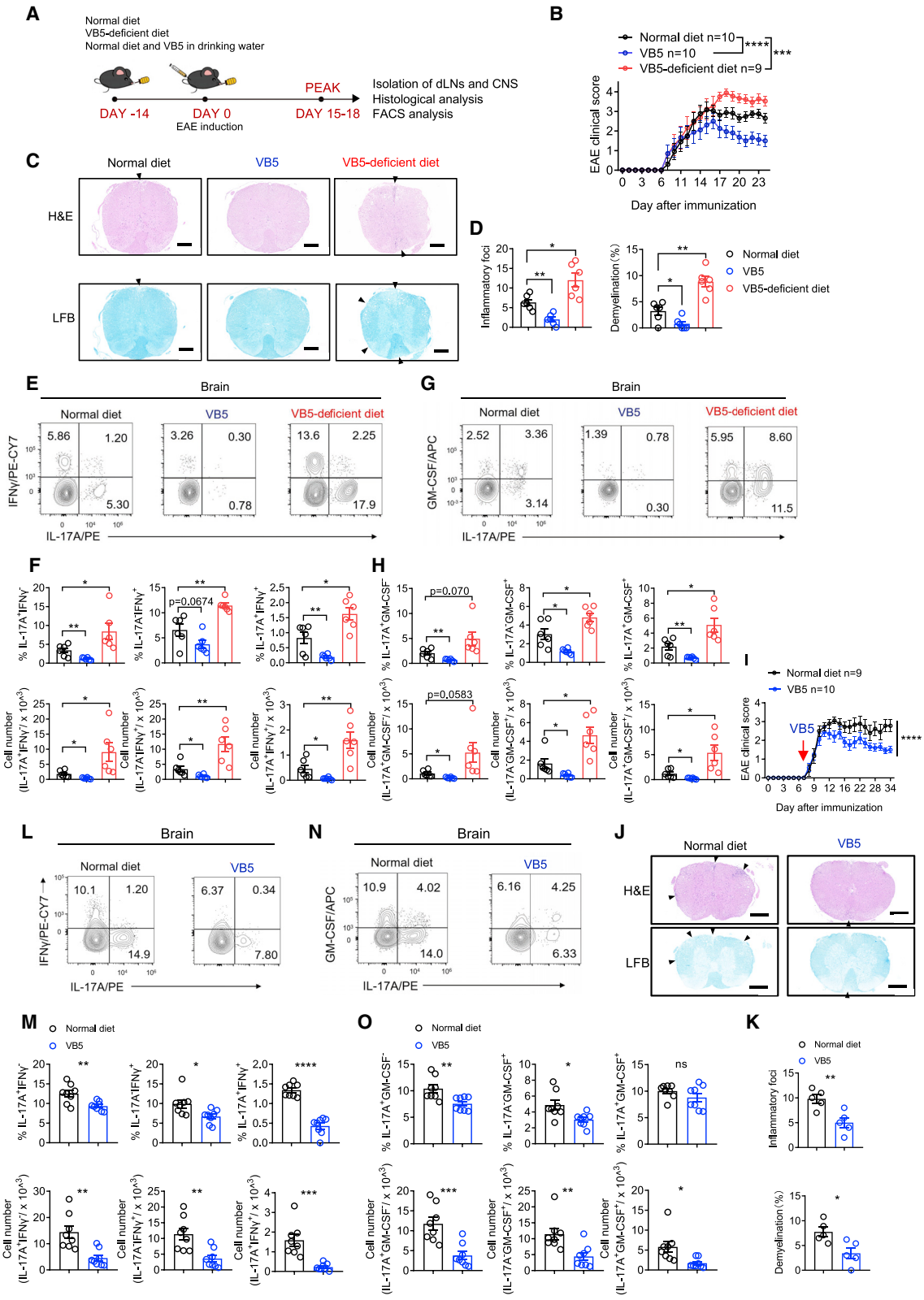
A
Normal diet
VB5-deficient diet
Normal diet and VB5 in drinking water
DAY -14
DAY 0
EAE induction
PEAK
DAY 15-18
Isolation of dLNs and CNS
Histological analysis
FACS analysis
B
Normal diet n=10
VB5 n=10
VB5-deficient diet n=9
EAE clinical score
Day after immunization
C
Normal diet
VB5
VB5-deficient diet
H&E
LFB
D
Inflammatory foci
Demyelination (%)
Normal diet
VB5
VB5-deficient diet
E
Brain
IFNγ/PE-CY7
IL-17A/PE
G
GM-CSF/APC
F
H
p=0.0674
p=0.070
p=0.0583
I
VB5
L
N
J
K
M
O
ns
(legend on next page)

We also used the naive $CD4^+$ T cell-transfer colitis model to compare mice given the normal diet with mice supplemented with additional VB5 in drinking water (Figure 1A). Compared with normal diet-fed mice, the mice with VB5 supplementation had a longer colon length (Figure 1C), a reduced extent of inflammation in spleen and mLN (Figure 1D), and had less severe epithelial damage in the colon (Figures 1E and 1F), reflecting milder colitis phenotype. Moreover, the VB5 supplementation significantly reduced the frequency and cell number of IL-17A-producing Th17 cells in both colon and mLN (Figures 1G–1J) compared with the normal diet-fed animals. In addition, VB5 supplementation also significantly reduced the frequency and cell number of IL-$17A^-$ IFNγ^+ $CD4^+$ T cells in both the colon and mLN (Figures 1G–1J). Similarly, mRNA expression of *Il17a*, *Ifng*, *Csf2*, *Il22*, and *Il23r* was downregulated, whereas *Il10* and *Foxp3* expression was significantly upregulated upon VB5 supplementation (Figure S2C).

To exclude the possibility that diet alone might affect body weight change, we fed *Rag1*$^{-/-}$ mice with a normal diet, a VB5-deficient diet, or a normal diet with VB5 supplementation in drinking water, without $CD4^+$ naive T cell transfer. Notably, we found no body weight loss in three treatments in *Rag1*$^{-/-}$ mice, indicating VB5 deficiency diet alone was not sufficient to elicit colitis (Figure S2D). These results indicated VB5 supplementation ameliorates colitis in mice with diminished IL-$17A^+$IFNγ^- and IL-$17A^-$ IFNγ^+ $CD4^+$ T cells in inflamed tissue, while VB5-deficiency renders mice prone to colitis, accompanied with more IL-$17A^+$IFNγ^- and IL-$17A^-$IFNγ^+ $CD4^+$ T cell infiltration.

Vitamin B5 alleviates experimental autoimmune encephalomyelitis

We next tested whether VB5 affects experimental autoimmune encephalomyelitis, another Th17-mediated autoimmune disease model. Mice were treated for 2 weeks with a normal diet, a VB5-deficient diet, or VB5 supplementation in drinking water before immunization with $MOG_{35–55}$ peptide in complete Freund's adjuvant to induce the EAE development (Figure 2A). We observed that the VB5-deficient diet treated mice showed higher EAE clinical scores and higher disease activity compared with normal diet-fed mice (Figures 2B and S3A). Consistently, in comparison with normal diet-fed mice, VB5-deficient diet-fed mice had more immune cell infiltration in spinal cords as measured by H&E staining, and increased demyelination as measured using Luxol fast blue (LFB) staining (Figures 2C and 2D). In contrast, VB5 supplementation significantly alleviated disease severity, accompanied with lower clinical scores and lower inflammatory cell infiltration and decreased demyelination in the spinal cord (Figures 2B–2D and S3A) compared with normal diet-treated mice.

Analysis of infiltrated immune cells in the central nerve system, including the spinal cord and the brain, showed that IL-$17A^+$ Th17 cells were significantly increased in the brain and spinal cord upon VB5-deficient diet treatment (Figures 2E–2H and S3B–S3F). In addition, VB5 deficiency also resulted in increased IL-$17A^-$IFNγ^+ and IL-$17A^-$GM-CSF^+ $CD4^+$ T cells in the brain (Figures 2E–2H). Conversely, VB5 supplementation significantly reduced IL-$17A^+$ Th17 cells, IL-$17A^-$IFNγ^+, and IL-$17A^-$GM-CSF^+ $CD4^+$ T cells in both spinal cord and brain (Figures 2E–2H and S3B–S3F). mRNA level of *Il17a*, *Csf2*, *Ifng*, *Il22*, *Tnf*, and *Il23r* in both brain and spinal cord were also upregulated in VB5-dificient diet but downregulated in VB5 supplementation (Figures S3G and S3H). In contrast, mRNA expression of *Il10* and *Foxp3* were downregulated in VB5-deficient diet but upregulated in VB5 supplementation (Figures S3G and S3H). The frequency of IL-$17A^+$ Th17 cells in the spleen and draining lymph node (dLN) were also reduced upon VB5 supplementation but augmented under a VB5-deficient context, although exhibiting a low percentage (Figures S3I and S3J). These observations indicate that VB5 supplementation mitigated neuroinflammation, and reduced pathogenic IL-$17A^+$ Th17 cells, IL-$17A^-$IFNγ^+ and IL-$17A^-$GM-CSF^+ $CD4^+$ T cells in spinal cord and brain, whereas VB5 deficiency rendered mice prone to EAE and endowed more pathogenic cells accumulation in the spinal cord and brain.

To determine whether VB5 supplementation can therapeutically alleviate EAE progression, we treated mice with VB5 in drinking water start on day 7 after disease onset. Of interest, we observed significant disease improvement showing by reduced EAE clinical score in mice fed with VB5 compared with normal diet-treated mice (Figure 2I). We also found obviously reduced immune cell infiltration and demyelination in the spinal cord under VB5 supplementation context (Figures 2J

Figure 2. VB5 supplementation ameliorates EAE, whereas VB5 deficiency accelerates EAE

(A) Schematic of the experimental design. C57BL/6 male mice (aged 6–8 weeks) were fed with normal diet/normal water, VB5-deficient diet/normal water, or normal diet/VB5 water for two weeks before immunization with $MOG_{35–55}$ to induce EAE.

(B) EAE clinical score of the indicated groups of mice (n = 9 or 10).

(C) Representative histology image of a spinal cord section with H&E (top) or Luxol fast blue (LFB) (bottom) staining in the indicated groups of mice (scale bars, 300 μm).

(D) Quantification of inflammatory foci and demyelination in indicated group (n = 6).

(E–H) Representative FACS plots (E and G) and quantification (F and H) showing percentage and absolute numbers of IL-$17A^+$IFNγ^-, IL-$17A^+$IFNγ^+, IL-$17A^-$IFNγ^+, IL-$17A^+$GM-CSF^-, IL-$17A^+$GM-CSF^+, IL-$17A^-$GM-CSF^+ $CD4^+$ T cells in the brain from indicated mice (n = 6).

(I–O) Therapeutic effect of VB5 to treat EAE. Mice were treated with VB5 (50 mg/kg/day) in drinking water at the onset of EAE (red arrow). EAE clinical score (n = 9 or 10) (I), representative H&E (top) and Luxol fast blue (LFB) (bottom) staining of spinal cord sections from indicated mice (scale bars, 400 μm) (J), quantification of inflammatory foci and demyelination in indicated group (n = 5) (K), representative FACS plots (L and N), and quantification (M and O) showing percentage and absolute numbers of IL-$17A^+$IFNγ^-, IL-$17A^+$IFNγ^+, IL-$17A^-$IFNγ^+, IL-$17A^+$GM-CSF^-, IL-$17A^+$GM-CSF^+, IL-$17A^-$GM-CSF^+ $CD4^+$ T cells in the brain from indicated mice (n = 8).

Data in (A)–(H) are representative of three independent experiments, and data in (I)–(O) are representative of two independent experiments. All data are mean ± SEM and were analyzed using the two-tailed, unpaired Student's t test (D, F, H, K, M, and O), two-way repeated-measures (RM) ANOVA (I), or two-way ANOVA with Tukey's multiple-comparisons test (B). *p < 0.05, **p < 0.01, ***p < 0.001, and ****p < 0.0001. See also Figure S3.

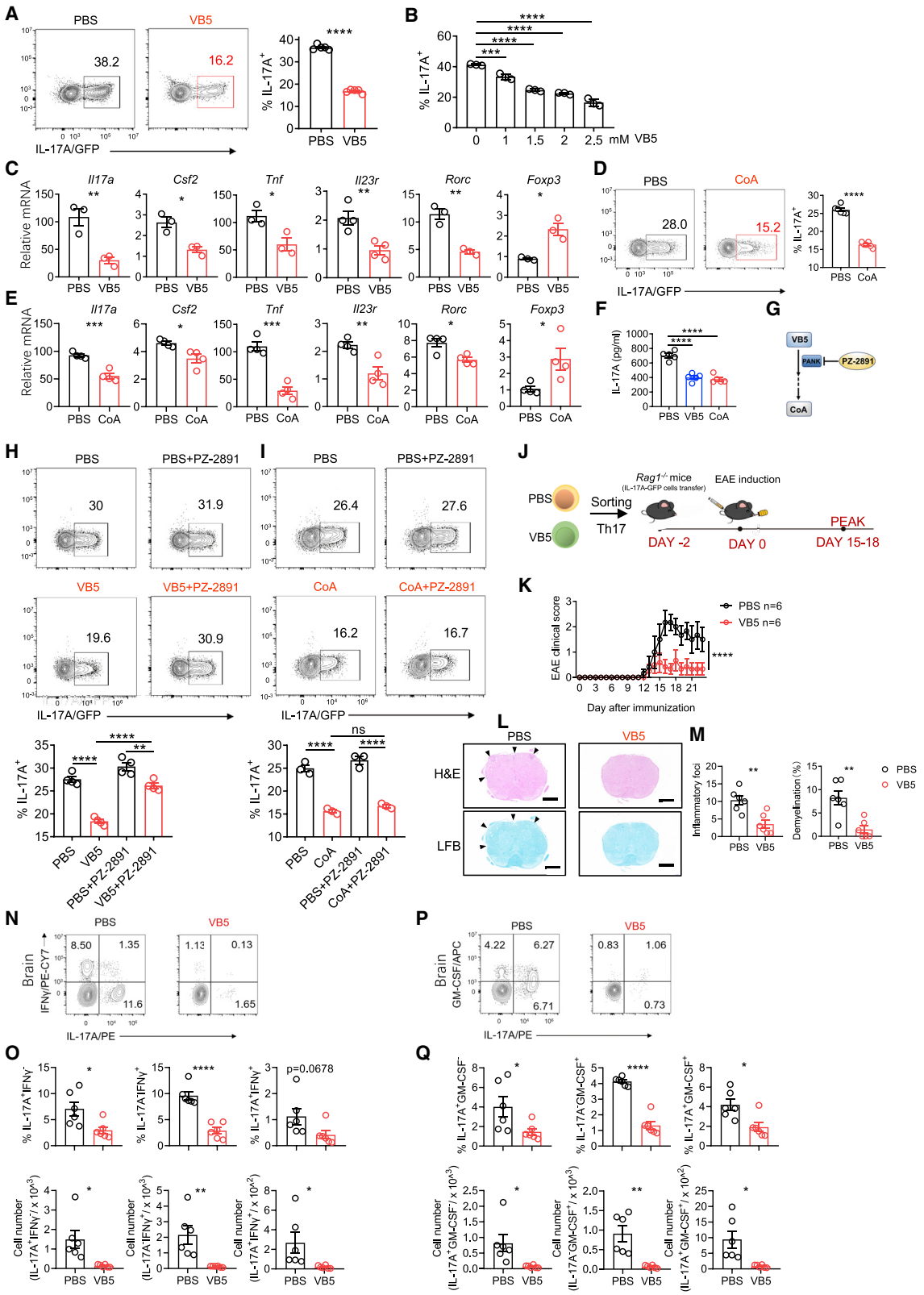

(legend on next page)

and 2K). The infiltrations of IL-17A$^+$ Th17 cells, IL-17A$^-$IFNγ^+ and IL-17A$^-$GM-CSF$^+$ CD4$^+$ T cells were significantly diminished in the brain upon VB5 supplementation (Figures 2L–2O). These data indicate the therapeutic potential of VB5 in treating human MS.

Vitamin B5 restrains Th17 cell differentiation through CoA in a PANK-dependent manner

On the basis of the *in vivo* models and *in vitro* screening results, we next sought to determine whether and how VB5 affects the activation, differentiation, and function of Th17 cells. We differentiated naive CD4$^+$ T cells into Th17 cells, with or without VB5, in culture medium for 96 h. We observed that the presence of VB5 dramatically decreased the extent of Th17 cell differentiation, doing so in a dose-dependent manner (Figures 3A, 3B, and S4A). The restraint of Th17 cell differentiation was also confirmed at the mRNA level: the VB5-exposed cells had significantly reduced expression of Th17-associated molecules *Il17a*, *Csf2*, *Tnf*, *Il23r*, and *Rorc*, but the expression of *Foxp3* was upregulated (Figure 3C). We examined whether this observed reduction in the extent of Th17 differentiation was influenced by inhibition of cell activation and proliferation. VB5 exposure did not affect cell viability, activation or proliferation under Th17-skewing conditions (Figures S4B–S4E). Thus, VB5 exposure restrains Th17 cell differentiation *in vitro* without affecting cell viability, activation, or proliferation.

VB5 is a precursor for the biosynthesis of coenzyme A (CoA); we do observe an increase of cellular CoA in T cells exposed to excessive VB5 (Figure S4F). We next explored the potential impact(s) of CoA on Th17 cell differentiation *in vitro*. We differentiated naive CD4$^+$ T cells under Th17-skewing conditions with or without CoA in the culture medium for 96 h. We found that CoA exposure significantly diminished the frequency of IL-17A-producing Th17 cells (Figure 3D). This inhibition of Th17 cell differentiation upon exposure to CoA was also confirmed at the mRNA level: CoA significantly reduced Th17-associated *Il17a*, *Csf2*, *Tnf*, *Il23r*, and *Rorc* expression (Figure 3E). Consistently, CoA exposure also promoted *Foxp3* expression in Th17 cells (Figure 3E). By measurement of IL-17A protein level in culture medium of differentiated Th17 cells, we found that VB5- or CoA-exposed cells had lower IL-17A secretion compared with PBS-exposed control cells (Figure 3F).

We also measured the effects of VB5 or CoA in other T helper cells, including Th1, Th2, and regulatory T (Treg) cell. Th1 cell differentiation was comparable upon VB5 or CoA treatment, compared with PBS control (Figures S4G and S4H). Although the differentiation of Th2 and Treg cells was significantly promoted by VB5 or CoA (Figures S4G and S4H). Together, these results indicated that VB5 or CoA specifically restrained Th17 but promoted Th2 and Treg cell differentiation *in vitro*.

Pantothenate kinase (PANK) is one of the enzymes that catabolize VB5 to CoA (Figure 3G). We next used PZ-2891, a reported PANK inhibitor, to test whether block the synthesis of CoA affects Th17 cell differentiation. We found that PZ-2891 treatment prevents VB5 exposure-induced inhibition of Th17 cell differentiation (Figure 3H). However, PZ-2891 treatment did not affect the inhibition of Th17 cell differentiation by CoA exposure (Figure 3I), indicating that the observed inhibition of Th17 cell differentiation resulting from exposure to VB5 is dependent on the enzymatic activity of PANK.

Vitamin B5 ameliorates Th17 cell-transfer-induced EAE

The finding that VB5 exposure restrains Th17 cell differentiation *in vitro* raised a question whether the VB5-treated Th17 cells are less potent to induce autoimmune disease *in vivo*. We used a Th17 cell adoptive transfer EAE model (Figure 3J). Briefly, we differentiated naive CD4$^+$ T cells into Th17 cells with or without VB5 treatment for 96 h. Differentiated IL-17A$^+$ Th17 cells were sorted and transferred into *Rag1*$^{-/-}$ mice, then recipient mice were immunized with $MOG_{35–55}$ peptide to induce EAE (Figure S4I). We observed that the mice received VB5-exposed Th17 cells exhibited a much lower EAE clinical score (Figure 3K), reduced inflammatory cell infiltration and demyelination in the

Figure 3. VB5 restrains Th17 differentiation through CoA in a PANK-dependent manner

(A) Representative FACS plots (left) and quantification (right) showing percentage of IL-17A-GFP on PBS or VB5 (2 mM) treated cells under Th17 differentiation conditions (n = 5).

(B) Quantification of IL-17A$^+$ cell percentage treated with 0, 1, 1.5, 2, or 2.5 mM VB5 (n = 3).

(C) qPCR analysis for the expression of indicated genes (percentage mRNA relative to *Hprt*) in Th17 cells treated with PBS or VB5 (n = 3).

(D) Representative FACS plots (left) and quantification (right) of PBS- or CoA (0.3 mM)-treated Th17 cells (n = 6).

(E) qPCR analysis for the expression of indicated genes (percentage mRNA relative to *Hprt*) in Th17 cells treated with PBS or CoA (n = 4).

(F) ELISA measurement of IL-17A protein levels in T cell supernatant treated with PBS, VB5 or CoA (n = 5).

(G) Schematic of VB5 catabolism.

(H and I) Representative FACS plot and quantification showing percentage of IL-17A$^+$ T cells treated with 10 μM PZ-2891 combined with VB5 (H) or CoA (I) (n = 4 or 3).

(J) Schematic of experimental design. Differentiated Th17 cells were treated with PBS or 2 mM VB5, then IL-17A-GFP cells were sorted and transferred intravenously into *Rag1*$^{-/-}$ mice (1 × 10^6 cells per mouse) and EAE was induced.

(K) EAE clinical score (n = 6).

(L) Representative staining with H&E (top) and Luxol fast blue (LFB) (bottom) of spinal cord sections from indicated mice (scale bars, 400 μm).

(M) Quantification of inflammatory foci and demyelination from indicated mice (n = 6).

(N–Q) Representative FACS plots (N and P) and quantification (O and Q) showing percentage and absolute numbers of IL-17A$^+$IFNγ^-, IL-17A$^+$IFNγ^+, IL-17A$^-$IFNγ^+, IL-17A$^+$GM-CSF$^-$, IL-17A$^+$GM-CSF$^+$, IL-17A$^-$GM-CSF$^+$ CD4$^+$ T cells in the brain from indicated mice (n = 6).

Data in (A)–(I) are representative of three independent experiments, and data in (J)–(Q) are representative of two independent experiments. All data are mean ± SEM and were analyzed using the two-tailed, unpaired Student's t test (A, C–E, M, O, and Q), one-way ANOVA with Dunnett's multiple-comparisons test (B and F), one-way ANOVA with Tukey's multiple-comparisons test (H and I), or two-way RM ANOVA (K). ns, not significant ($p > 0.05$). *$p < 0.05$, **$p < 0.01$, ***$p < 0.001$, ****$p < 0.0001$. See also Figure S4.

spinal cord compared with mice that received PBS-exposed Th17 cells (Figures 3L and 3M).

Further analysis of infiltrated immune cells in the brain and spinal cord showed that mice received VB5-exposed Th17 cells had much lower GM-CSF and IFNγ expression (Figures 3N–3Q and S4J–S4M), both cytokine that are important in Th17 induced pathogenesis.[35] These data suggested that VB5-exposed Th17 cells were intrinsically less potent to elicit autoimmune disease.

Vitamin B5 dampens glucose metabolism during Th17 cell differentiation

To determine the underlying mechanisms of VB5-mediated regulation of Th17 cell differentiation, we performed RNA sequencing (RNA-seq) comparing VB5- or PBS-treated Th17 cells at 48 h post-treatment. We observed that global changes in gene expression are induced by VB5 treatment (Figure S5A). Consistent with the observation that VB5-exposed Th17 cells are less pathogenic (Figures 3J–3Q), gene set enrichment analysis (GSEA) using previously defined Th17 signature also revealed that VB5-exposed Th17 cells are less pathogenic compared with PBS treatment[36] (Figures S5B and S5C). Of note, the VB5-exposed cells had significantly decreased expression of multiple carbohydrate metabolism associated genes (Figure 4A). This finding motivated us to investigate whether VB5 exposure affects glucose metabolism in Th17 cells. We next performed seahorse analysis of VB5- or PBS-exposed $CD4^+$ T cells, which is under Th17-skewing conditions, and found that VB5 exposure significantly impaired glycolysis in these cells, as measured by extracellular acidification rate (ECAR) (Figures 4B and 4C). Also, we observed that VB5 treatment inhibited oxidative phosphorylation (OXPHOS), as measured by oxygen consumption rate (OCR), in terms of both spare respiration capacity and maximal respiration (Figures S5D and S5E). Consistently, treatment with CoA also significantly reduced glycolysis (Figures 4D and 4E), as well as OXPHOS (Figures S5F and S5G) in Th17 cells. Indeed, consistent with reduced OXPHOS, VB5- or CoA-treated Th17 cells both displayed disrupted mitochondria function, as measured by mitochondrial mass (Figures S5H and S5I), and ROS production (Figures S5J and S5K). Furthermore, we used metabolomics profiling to evaluate potential effects of VB5-mediated metabolic regulation. In consistent with the RNA-seq and ECAR/OCR results, we observed that VB5 exposure led to significant reduction of fructose-6-phosphate (F6P), and TCA cycle intermediates (e.g., *cis*-aconitate and malate) (Figures 4F–4H). These findings support that exposure to VB5 or elevated CoA levels inhibits the glucose metabolism during Th17 cell differentiation.

CoA binds to PKM2 and impedes its nuclear translocation

We next wanted to interrogate the cellular mechanisms underlying VB5/CoA inhibiting Th17 cell differentiation. Given that CoA is a co-factor for cellular biochemical reaction, we are curious whether CoA may directly associate with an enzyme to regulate glucose metabolism. We used a CoA-immobilized agarose (CoA-agarose) to incubate with protein lysates of splenocytes, then the extracts from samples that were pulled down by CoA-agarose, or the gel bands were submitted to liquid chromatography/mass spectrometry (LC/MS) analysis, only one promising binding partner, pyruvate kinase 2, was found to be associated with CoA (the top 10 candidates for both conditions are hown in Table S1) (Figures 5A and S6A). We then validated the interaction between PKM2 and CoA by immunoprecipitation (IP)/western blot (WB), the immunoblotting showed that CoA strongly interacted with endogenous PKM2 (Figure 5B). PKM2 is a multifunctional protein existing various different states, including monomeric, dimeric, and tetrameric states.[37] Tetrameric PKM2 exhibit glycolytic enzyme activity, redundant with PKM1, whereas dimeric/monomeric PKM2 are less enzymatic and can translocate into nucleus as a transcriptional coactivator.[22] Of note, the expression of *Pkm2* was induced during Th17 differentiation, while the expression of *Pkm1* was very low in Th17 cells, indicating a dominant role of PKM2 in Th17 differentiation (Figure 5C). Indeed, PKM2 but not PKM1 was reported to be involved in Th17 differentiation.[23,25]

In agreement with a previous study showing that PKM2 affects glycolysis by stabilizing HIF1α in the nucleus,[22] we found CoA exposure significantly reduced the expression of HIF1α-targeted glycolytic enzyme genes such as *Tpi1*, *Pgam1*, *Pgk1*, and *Hk2* during Th17 differentiation (Figure 5D), In addition, nuclear PKM2 was shown to bind to and enhance STAT3 phosphorylation during Th17 cell differentiation.[23] Supporting that, we found the nuclear phosphorylated STAT3 is significantly reduced in VB5- or CoA-exposed Th17 cells compared with PBS-treated Th17 cells (Figure 5E). Thus, VB5 or CoA likely regulates the nucleic function of PKM2. As the monomeric, dimeric, and tetrameric states of PKM2 are important for its nuclear translocation,[37] we reasoned whether VB5 or CoA could impede PKM2 nuclear translocation via regulating the monomeric, dimeric, and tetrameric states of PKM2. We collected VB5- or CoA-exposed Th17 cells at different time points for immunoblotting of PKM2 or Y105 phosphorylation of PKM2, a modification represses tetrameric PKM2 formation and promote PKM2 nuclear localization.[38] VB5 exposure significantly increased the level of tetrameric PKM2 and significantly decreased the monomeric PKM2 level at 48 and 72 h of Th17 cell differentiation (Figure 5F). In addition, VB5- or CoA-exposed Th17 cells displayed significantly diminished PKM2 Y105 phosphorylation (Figures 5G and 5H). Consistently, we also observed significantly reduced nuclear PKM2 upon exposure to VB5 or CoA (Figure 5E). These data suggested that CoA inhibits HIF1α-regulated glucose metabolism and reduces nuclear STAT3 phosphorylation during Th17 differentiation, through preventing the phosphorylation, and nuclear translocation of PKM2 in Th17 cells.

To verify whether PKM2 plays an important role in VB5-mediated suppression of autoimmune disease models, we used a small-molecule PKM2 activator, TEPP-46, which inhibits the phosphorylation and nuclear translocation of PKM2, to test whether targeting PKM2 reverse the severe EAE phenotype upon feeding with VB5-deficient diet (Figure 5I). We found that TEPP-46 (dissolved in PEG300) treatment reverses the severe EAE phenotype upon feeding with VB5-deficient diet, exhibiting no difference of mean EAE clinical score, immune cell infiltration, and extent of demyelination in the spinal cord from mice treated with VB5-deficient diet/TEPP-46 compared with normal diet/TEPP-46 (Figures 5J–5L). As a control, PEG300 treatment did

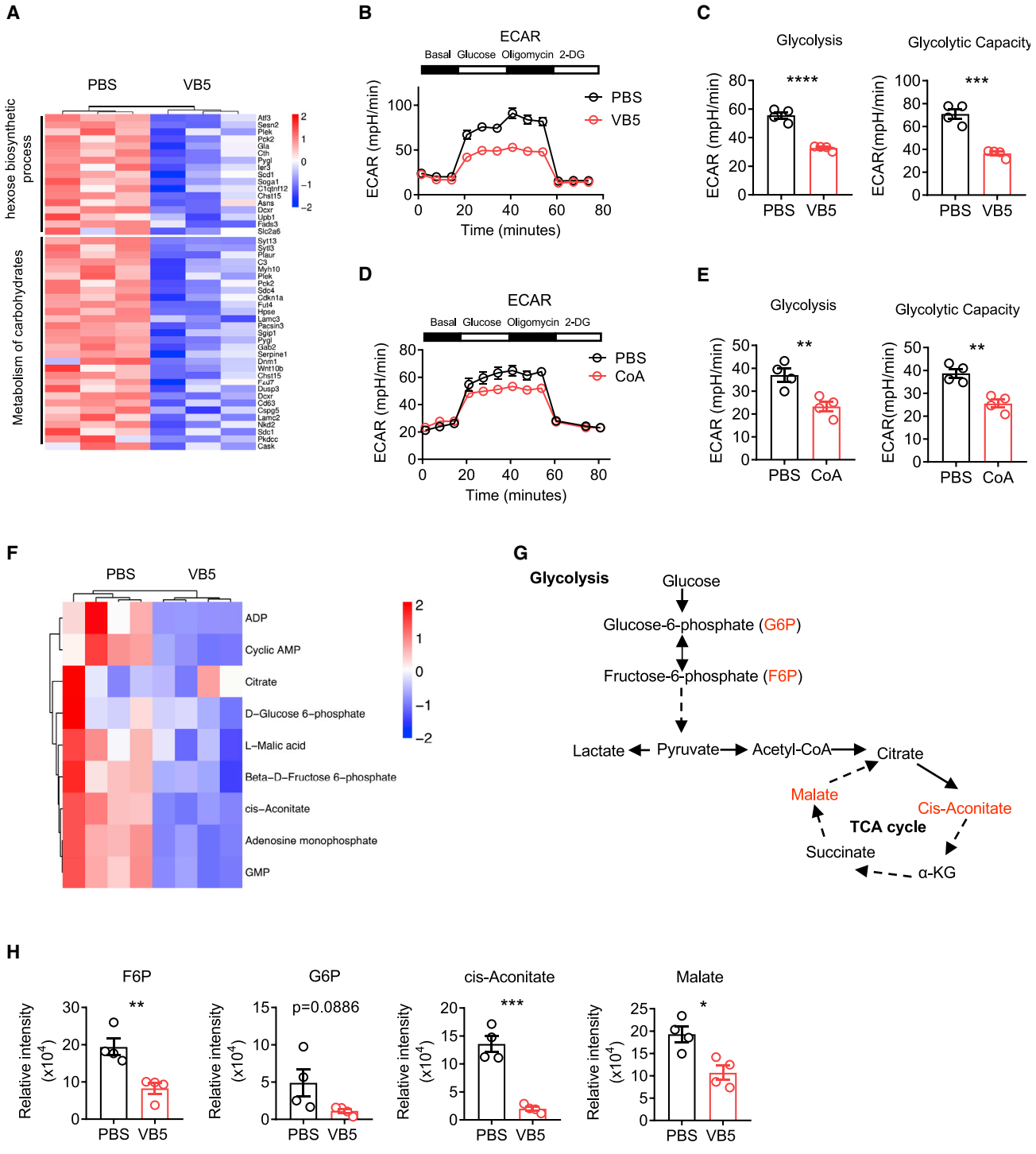

Figure 4. VB5 inhibits glucose metabolism during Th17 differentiation

Naive CD4$^+$ T cells were polarized under Th17 (IL-6$^+$TGF-β1$^+$IL-23) culture conditions for 48 h in combination with VB5, CoA, or PBS treatment.

(A) Heatmap of RNA sequencing data from differentiated Th17 cells treated with PBS or VB5 *in vitro*.

(B–E) Naive CD4$^+$ T cells were differentiated under Th17 conditions in the presence of VB5, CoA, or PBS. Seahorse experiments showing extracellular acidification rate (ECAR) of *in vitro* differentiated Th17 cell treated with VB5 (B and C) or CoA (D and E).

(F–H) Naive CD4$^+$ T cells were treated with VB5 or PBS for 48 h under Th17-skewing conditions. Heatmap of metabolites analyzed by LC/MS in the energy metabolism pathways (F), summary of indicated metabolites from the glucose metabolism pathways (G), and quantification of metabolites (H) (n = 4).

Data in (B)–(E) are representative of three independent experiments. All data are mean ± SEM and were analyzed using the two-tailed, unpaired Student's t test (C, E, and H). *p < 0.05, **p < 0.01, and ***p < 0.001. See also Figure S5.

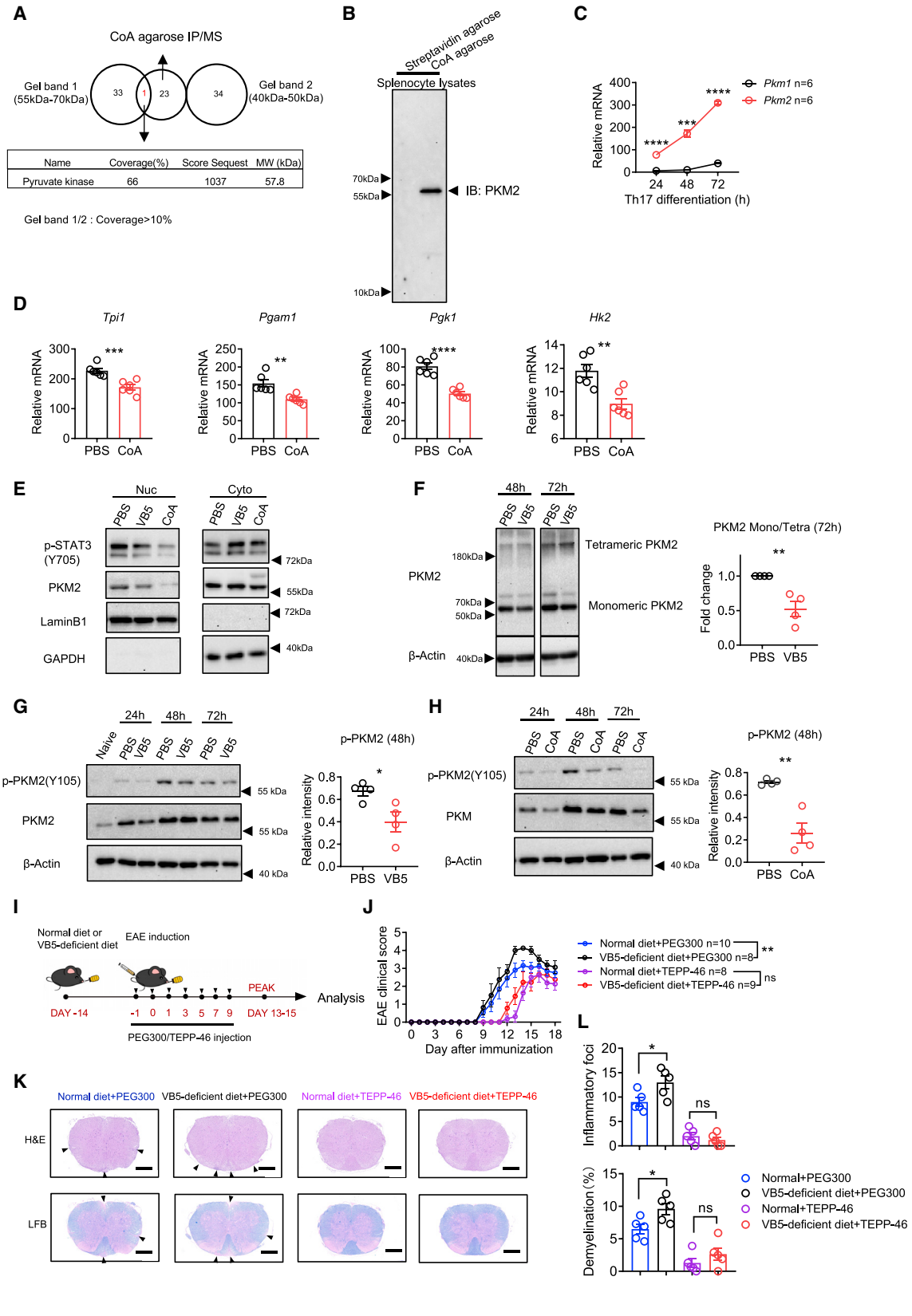

(legend on next page)

not reverse the severe EAE phenotype (Figures 5J–5L). Collectively, these findings suggested that VB5 suppresses Th17 differentiation and EAE development, likely through modulating PKM2 function.

Vitamin B5 inhibits human Th17 cell metabolism and is reduced in the serum of UC and MS patients

We next investigated the potential impact of VB5 on human Th17 cell differentiation, as well as the serum VB5 levels in human autoimmune diseases, such as IBD and MS. We first differentiated human naive $CD4^+$ T cells under human Th17-skewing conditions.[39] Similar to mouse Th17 cells, we found VB5 or CoA exposure significantly reduced human Th17 cell differentiation, as revealed by decreased frequency of IL-17A-producing $CD4^+$ T cells (Figures 6A, 6B, and S7A), as well as reduced mRNA levels of Th17-associated genes (Figures 6C and 6D). We also measured human Th17 cell glucose metabolism upon exposure to CoA. In comparison with the PBS-treated group, CoA treatment resulted in reduced cellular glucose metabolism as measured by ECAR (Figures 6E and 6F) and OCR (Figures S7B and S7C). In consistent with our data in mouse Th17 cells, VB5 or CoA exposure also increased PKM2 tetramerization (Figure 6G), decreased PKM2 Y105 phosphorylation and nuclear translocation of PKM2 (Figures 6H and 6I). These data suggest a conserved regulatory mechanism of Th17 cell glucose metabolism by VB5/CoA/PKM2.

A recent study of the Integrative Human Microbiome Project revealed that the VB5 level was particularly low in the gut of IBD patients, suggesting a potential correlation between VB5 reduction and IBD development.[37] However, whether VB5 levels are also decreased in other autoimmune diseases and whether VB5 levels correlates with impaired Th17 function is unknown. Thus, we measured the levels of VB5 and IL-17A in the serum of autoimmune disease patients, such as IBD and MS. Compared with healthy controls, the serum VB5 levels are significantly reduced in ulcerative colitis (UC) patients and MS patients (Figures 6J and 6K, Table S2). Conversely, the serum IL-17A levels are significantly higher in UC patients or MS patients, in comparison with the healthy controls (Figures 6J and 6K). Furthermore, we confirmed the serum VB5 level was significantly reduced in colitis mice, in comparison with healthy controls (Figure S7D). We then sought to determine the potential mechanism of the VB5 deficiency. One of the hypotheses is that the transporter of VB5 (SLC5A6) may decrease in mice received $CD45RB^{hi}$ T cell transfer. Of note, we found that the mRNA level of *Slc5a6* was significantly decreased in inflamed colon from mice received $CD45RB^{hi}$ T cell transfer (Figure S7E). Besides, the decrease of *Slc5a6* was also found in the inflamed colon from other mouse inflammatory disease models such as dextran sulfate sodium (DSS)-induced colitis, *C. rodentium* infection, and TNF-α overexpression ($TNF^{\Delta ARE}$) models that mimic human Crohn disease (Figures S7F–S7H). These results implicated VB5 deficiency was common in autoimmune diseases, including UC and MS, and serum VB5 reduction might be a risk factor for IBD and MS.

DISCUSSION

Diet is well recognized as an important regulator for mediating host immune responses.[40] Particularly, dietary pattern shifts toward high sugar, high salt, and high fat have been demonstrated to exacerbate autoimmune diseases, specifically by favoring pathogenic Th17 cell differentiation,[29–31,41] which are known to be regulated by the inflammatory cytokine milieu and by metabolic reprogramming.[12,36,42,43] However, it is unclear whether diet can directly regulate Th17 cell function through metabolic reprogramming in autoimmune diseases.

Metabolic reprogramming is a hallmark of effector $CD4^+$ T helper cells, distinguishing them from, for example, naive and regulatory T cells. Th17 cells harness aerobic glycolysis to fulfill their needs for rapid activation and differentiation.[17] Recent studies have focused on dietary regulation of Th17 cell function (e.g., high salt/glucose), and revealed that high salt and high glucose content in the diet can promote inflammatory Th17 cell function: high salt causes transcriptional network changes, and high glucose causes altered cytokine signaling.[29,30] Another study that examined a high fat diet (HFD)-induced obesity model and reported that HFD-driven inflammatory Th17 cell pathology due to upregulation of the acetyl-CoA carboxylase 1 (ACC1) enzyme, which facilitates fatty acid synthesis.[31]

To the best of our knowledge, there are no studies link dietary intake and Th17 cell metabolism. Our data show that VB5

Figure 5. CoA binds to PKM2 and impedes its nuclear translocation

(A) Splenocyte lysates were incubated with CoA-agarose for 2 h, followed by immunoprecipitation of the CoA-agarose complexes and LC/MS analysis.

(B) Western blotting detection of endogenous PKM2 immunoprecipitated by CoA.

(C) Real-time qPCR data of *Pkm1* and *Pkm2* mRNA expression (percentage mRNA relative to *Hprt*) at the indicated time point during Th17 cell differentiation (n = 6).

(D) Real-time qPCR data of *Tpi1*, *Pgam1*, *Pgk1*, and *Hk2* mRNA expression (percentage mRNA relative to *Hprt*) in Th17 cells at 48 h treated with PBS or CoA (n = 6).

(E) Western blotting showing PKM2 nuclear translocation and STAT3 phosphorylation treated with VB5 or CoA.

(F) Cells were subjected to protein cross-linking using disuccinimidyl suberate (DSS) followed by immunoblot analysis to identify PKM2 oligomer states at different time points of Th17 cell differentiation.

(G and H) Western blotting detection of PKM2 phosphorylation treated by VB5 (G) or CoA (H) at different time point of Th17 cell differentiation.

(I–L) Mice fed a diet deficient in VB5 or a normal diet were induced to develop EAE, then mice were treated every other day from day −1 to day +9 post-immunization with PEG300 or TEPP-46 30 mg/kg in PEG300 (I), EAE clinical score (J), representative H&E (top), and Luxol fast blue (LFB) (bottom) staining of spinal cord sections from indicated mice (scale bars, 400 μm) (K), quantification of inflammatory foci and demyelination from indicated mice (L) (n = 5).

Data in (B)–(H) are representative of three independent experiments. Data in (I)–(L) are representative of two independent experiments. All data are mean ± SEM and were analyzed using the two-tailed, unpaired Student's t test (D, F–H, and L), two-way ANOVA with Sidak's multiple-comparisons test (C), or two-way ANOVA with Tukey's multiple-comparisons test (J). ns, not significant ($p > 0.05$). *$p < 0.05$, **$p < 0.01$, ***$p < 0.001$, and ****$p < 0.0001$. See also Figure S6 and Table S1.

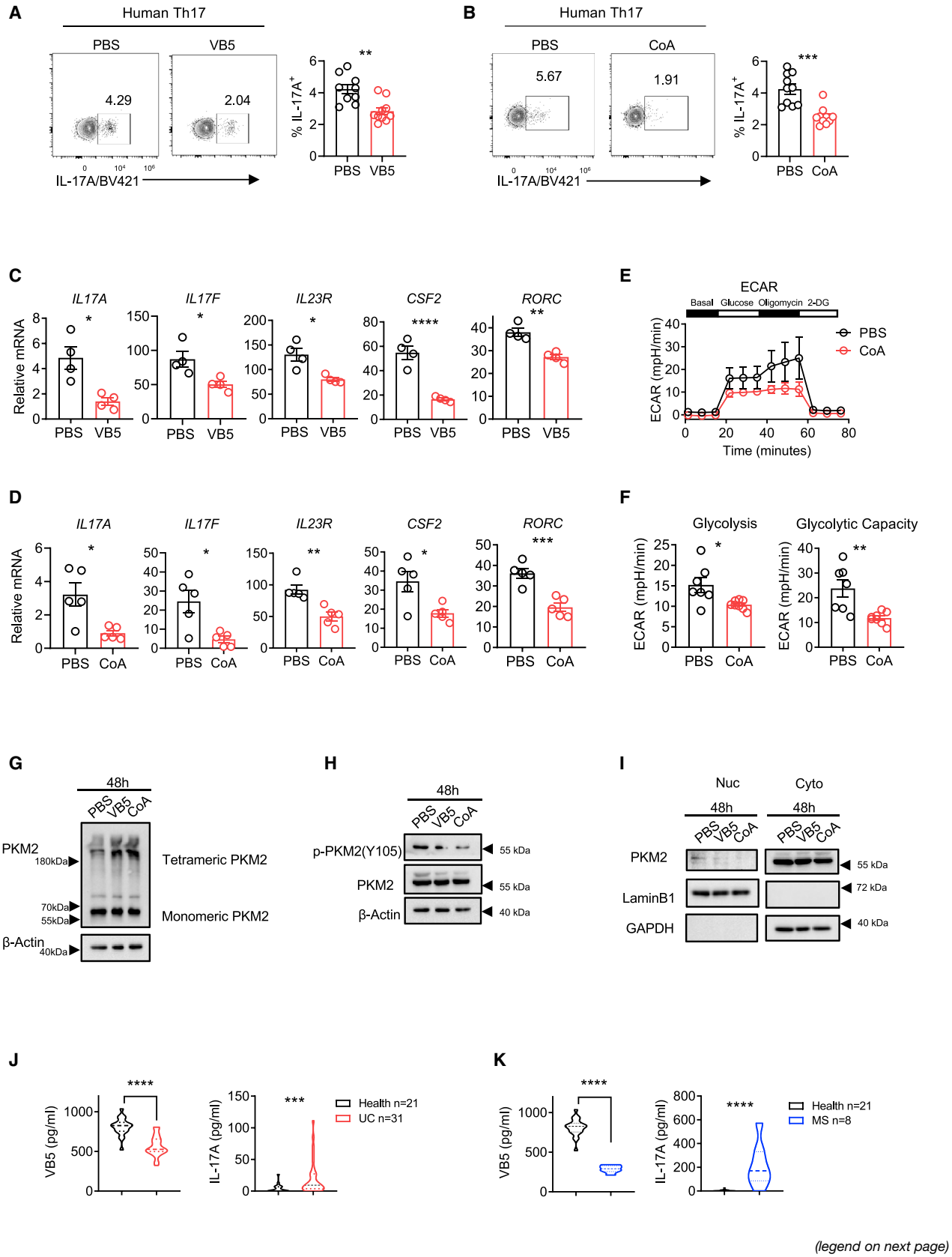

(legend on next page)

restrains Th17 cell differentiation by inhibiting glycolysis and STAT3 phosphorylation. Considering that intracellular VB5 is the precursor for production of coenzyme A, for the first time, we identified CoA is a ligand of the glycolytic enzyme PKM2. A recent study demonstrated that PKM2-dependent metabolic skewing affects Th17 cell function in an inflammatory context. Moreover, a so-called moonlighting activity of PKM2 has been documented, wherein monomeric/dimeric PKM2 translocate into nucleus and functions as a coactivator to maintain HIF1α transcriptional activity.[22] A previous study also showed that treatment of cultured Th17 cells with the allosteric modulator TEPP-46 inhibited both PKM2 nuclear translocation and glycolysis.[25] In addition, nuclear PKM2 was shown to bind to and enhance the extent of STAT3 phosphorylation throughout Th17 cell differentiation.[23]

In agreement with these studies, we showed that exposing to VB5 or CoA impedes PKM2 nuclear translocation and inhibits nuclear STAT3 phosphorylation, and VB5 and CoA exposure also disrupted glycolysis and OXPHOS during Th17 cell differentiation. During pyruvate oxidation, an acetyl group is attached to CoA to form acetyl-CoA, which is involved in the TCA cycle. We originally speculated that elevated intracellular CoA levels may favor the TCA cycle, but we observed that CoA exposure actually reduced OXPHOS. This might be because (1) CoA controls cellular metabolism in a context-dependent manner, and (2) CoA may exert "moonlighting" function outside of its role as an acyl group carrier. Indeed, we found that intracellular CoA functions as a ligand of PKM2 and impedes both PKM2 nuclear translocation and PKM2's nuclear function. We have also discussed the alternative possibilities of the mechanism: (1) given that CoA is important for the biosynthesis of fatty acid, elevated CoA in Th17 cells may participate in the biosynthesis of endogenous ligand of RORγt to direct Th17 cell differentiation, or (2) CoA acts as an acyl carrier, which has been well documented, and acetyl-CoA may provide acetyl group onto lysine residues of histone and non-histone proteins to regulate the transcription of Th17 related genes.

There are reports of using a neutralizing antibody against IL-17A, the hallmark of Th17 cells, to therapeutically intervene the Th17 cell-mediated autoimmune diseases. The efficiency of the antibody targeting IL-17A was impressive for psoriasis but was disappointing in Crohn disease and rheumatoid arthritis.[44–46] The neutralizing monoclonal antibody (mAb) targeting IL-17A even worsened the disease and caused severe side effects in Crohn disease.[45,47] Notably, previous studies have shown that an inflammatory milieu contains Th17 cells that are distinct from Th17 cells induced by homeostatic commensal bacteria, with obvious differences in their respective cellular metabolism.[15] Targeting the metabolic reprogramming of Th17 cells might represent an alternative therapeutic intervention for treating Th17 cell-mediated autoimmune diseases, such as IBD and MS. Although it has been demonstrated that inhibiting glycolysis and OXPHOS can effectively inhibit $CD4^+$ T cell activation and differentiation,[17,48,49] this approach is therapeutically intractable because of the required housekeeping function of glycolysis in many cell types. Indeed, inhibition of glycolysis with 2-DG caused the severe side effect of cytotoxicity.[50]

We show that VB5 metabolically reprograms Th17 cells in a manner that fine-tunes glycolysis and OXPHOS, and we demonstrated the therapeutic potential of exploiting this VB5-mediated reprograming of Th17 cells for treating EAE. Mice given VB5 had significantly reduced EAE clinical scores and inflammation in the CNS or colon. Our data also show that VB5 deficiency renders mice prone to EAE and colitis. In humans, patients with IBD and MS have significantly reduced serum VB5 levels compared with healthy controls. In agreement with the functional relevance of VB5 in IBD, a study from the Integrative Human Microbiome Project demonstrated VB5 depletion in the gut in IBD.[37] It is known that VB5 can be obtained from the diet and from commensal bacteria, so further investigations could perhaps distinguish specific autoimmune-related contributions from diet-versus microbiota-derived VB5. Collectively, our study links diet with metabolic reprogramming during the differentiation of inflammatory Th17 cells and illustrates that VB5 supplementation may represent a promising therapeutic intervention for Th17 cell-associated autoimmune diseases.

Limitations of the study

In our *in vitro* study, inhibition of PANK with PZ-2891 did not completely rescue the restraint of Th17 cell differentiation by VB5 (Figure 3H); additional evidence is necessary to demonstrate whether this is due to the efficacy of inhibitor or other CoA-independent pathways mediated by VB5.

VB5 was shown to be low in the gut of IBD patients in a recent study of the Integrative Human Microbiome Project,[37] and we also confirmed the decrease of VB5 in both IBD and MS patients (Figures 6J and 6K). In both human and mouse, VB5 originated from either diet or commensal bacteria; in addition, we found that the VB5 transporter SLC5A6 in the intestine is decreased during inflammation (Figures S7D–S7H). Whether dysregulated

Figure 6. VB5 inhibits human Th17 cell metabolism and is reduced in the serum of UC and MS patients

(A–D) Human naive $CD4^+$ T cells were differentiated under human Th17-skewing conditions and treated with VB5, CoA, or PBS for 7 days. Representative FACS plots and quantification treated with VB5 (A) (n = 9 or 10) or CoA (B) (n = 10), qPCR analysis of Th17-associated genes (percentage mRNA relative to *HPRT*) treated with VB5 (C) (n = 4) or CoA (D) (n = 5).

(E and F) Human naive $CD4^+$ T cells were differentiated under Th17 conditions in the presence of CoA or PBS, and ECAR was measured at 48 h (n = 7 or 8).

(G) Cells underwent protein cross-linking using disuccinimidyl suberate (DSS) followed by immunoblot analysis to identify PKM2 oligomer states at 48 h of Th17 cell differentiation treated with VB5 or CoA.

(H) Western blotting showing PKM2 phosphorylation treated by VB5 or CoA at 48 h of Th17 cell differentiation.

(I) Western blotting showing PKM2 nuclear translocation treated with VB5 or CoA at 48 h of Th17 cell differentiation.

(J) VB5 or IL-17A concentration in serum from recently diagnosed, untreated individuals with ulcerative colitis or healthy controls assayed using ELISA.

(K) VB5 or IL-17A concentration in serum from recently diagnosed, untreated individuals with multiple sclerosis and healthy controls assayed using ELISA.

Data in (A)–(F) are representative of three independent experiments. All data are mean ± SEM and were analyzed using the two-tailed unpaired Student's t test (A–D, F, J, and K). *$p < 0.05$, **$p < 0.01$, ***$p < 0.001$, and ****$p < 0.0001$. See also Figure S7 and Table S2.

dietary habit or dysbiosis of the microbiota contributes to VB5 loss in autoimmune diseases may need further investigation. Also, it is of interest to discriminate the immune-regulatory role of diet- versus bacteria-derived VB5 in pathophysiological conditions (e.g., IBD).

STAR★METHODS

Detailed methods are provided in the online version of this paper and include the following:

- KEY RESOURCES TABLE
- RESOURCE AVAILABILITY
  - Lead contact
  - Materials availability
  - Data and code availability
- EXPERIMENTAL MODEL AND SUBJECT DETAILS
  - Human subjects
  - Mice
  - Cell culture
- METHOD DETAILS
  - T cell–transfer colitis
  - EAE induction
  - T cell activation, differentiation, and proliferation *in vitro*
  - Isolation of lymphocytes from the lamina propria, spinal cord, and lymph nodes
  - Flow cytometry
  - Real-time PCR
  - H&E staining and LFB staining
  - Metabolism assays
  - LC/MS analysis
  - Immunoprecipitation
  - Cross-linking reaction and western blotting
  - Quantification and statistical analysis

SUPPLEMENTAL INFORMATION

Supplemental information can be found online at https://doi.org/10.1016/j.celrep.2022.111741.

ACKNOWLEDGMENTS

We thank Minghui Shi for help with some experiments. We thank Naizhong Hu and Na Hong for providing human IBD serum samples. We thank Zihao Li for providing human MS serum samples. This work was supported by grants from the National Key R&D Program of China (2020YFA0509101 to W.J. and 2018YFA0508000 to S.Z.), the Strategic Priority Research Program of the Chinese Academy of Sciences (XDB29030101 to S.Z.), the CAS Project for Young Scientists in Basic Research (YSBR-074), and the National Natural Science Foundation of China (82061148013, 91842105, and 81821001 to S.Z.; 82171783 and 81871284 to H.M.).

AUTHOR CONTRIBUTIONS

S.Z., C.C., and W.Z. conceived the project; C.C. and W.Z. performed most of the experiments and analyzed the data; Z.H. and W.J. analyzed VB5 levels using mass spectrometry; T.Z. analyzed the RNA sequencing data; Q.L., Q.M., S.C., and K.Z. provided human IBD samples; C.H. and C.Z. provided human MS samples; W.J., R.Z., W.P., and H.M. provided comments and suggestions; C.C., W.Z., and S.Z. wrote the manuscript; S.Z. supervised the project.

DECLARATION OF INTERESTS

S.Z., C.C., and W.Z. have filed a patent application on the role of vitamin B5 in the intervention of Th17-associated autoimmune diseases.

Received: March 8, 2022
Revised: September 21, 2022
Accepted: November 7, 2022
Published: November 29, 2022

REFERENCES

1. Park, H., Li, Z., Yang, X.O., Chang, S.H., Nurieva, R., Wang, Y.H., Wang, Y., Hood, L., Zhu, Z., Tian, Q., and Dong, C. (2005). A distinct lineage of CD4 T cells regulates tissue inflammation by producing interleukin 17. Nat. Immunol. *6*, 1133–1141. https://doi.org/10.1038/ni1261.
2. Harrington, L.E., Hatton, R.D., Mangan, P.R., Turner, H., Murphy, T.L., Murphy, K.M., and Weaver, C.T. (2005). Interleukin 17-producing CD4+ effector T cells develop via a lineage distinct from the T helper type 1 and 2 lineages. Nat. Immunol. *6*, 1123–1132. https://doi.org/10.1038/ni1254.
3. Langrish, C.L., Chen, Y., Blumenschein, W.M., Mattson, J., Basham, B., Sedgwick, J.D., McClanahan, T., Kastelein, R.A., and Cua, D.J. (2005). IL-23 drives a pathogenic T cell population that induces autoimmune inflammation. J. Exp. Med. *201*, 233–240. https://doi.org/10.1084/jem.20041257.
4. Ivanov, I.I., McKenzie, B.S., Zhou, L., Tadokoro, C.E., Lepelley, A., Lafaille, J.J., Cua, D.J., and Littman, D.R. (2006). The orphan nuclear receptor RORgammat directs the differentiation program of proinflammatory IL-17+ T helper cells. Cell *126*, 1121–1133. https://doi.org/10.1016/j.cell.2006.07.035.
5. Veldhoen, M., Hocking, R.J., Atkins, C.J., Locksley, R.M., and Stockinger, B. (2006). TGFbeta in the context of an inflammatory cytokine milieu supports de novo differentiation of IL-17-producing T cells. Immunity *24*, 179–189. https://doi.org/10.1016/j.immuni.2006.01.001.
6. Eming, S.A., Wynn, T.A., and Martin, P. (2017). Inflammation and metabolism in tissue repair and regeneration. Science *356*, 1026–1030. https://doi.org/10.1126/science.aam7928.
7. Stockinger, B., and Omenetti, S. (2017). The dichotomous nature of T helper 17 cells. Nat. Rev. Immunol. *17*, 535–544. https://doi.org/10.1038/nri.2017.50.
8. Kumar, P., Monin, L., Castillo, P., Elsegeiny, W., Horne, W., Eddens, T., Vikram, A., Good, M., Schoenborn, A.A., Bibby, K., et al. (2016). Intestinal interleukin-17 receptor signaling mediates reciprocal control of the gut microbiota and autoimmune inflammation. Immunity *44*, 659–671. https://doi.org/10.1016/j.immuni.2016.02.007.
9. Mao, K., Baptista, A.P., Tamoutounour, S., Zhuang, L., Bouladoux, N., Martins, A.J., Huang, Y., Gerner, M.Y., Belkaid, Y., and Germain, R.N. (2018). Innate and adaptive lymphocytes sequentially shape the gut microbiota and lipid metabolism. Nature *554*, 255–259. https://doi.org/10.1038/nature25437.
10. McGeachy, M.J., Cua, D.J., and Gaffen, S.L. (2019). The IL-17 family of cytokines in health and disease. Immunity *50*, 892–906. https://doi.org/10.1016/j.immuni.2019.03.021.
11. Gaffen, S.L., Jain, R., Garg, A.V., and Cua, D.J. (2014). The IL-23-IL-17 immune axis: from mechanisms to therapeutic testing. Nat. Rev. Immunol. *14*, 585–600. https://doi.org/10.1038/nri3707.
12. Geltink, R.I.K., Kyle, R.L., and Pearce, E.L. (2018). Unraveling the complex interplay between T cell metabolism and function. Annu. Rev. Immunol. *36*, 461–488. https://doi.org/10.1146/annurev-immunol-042617-053019.
13. Pearce, E.L., and Pearce, E.J. (2013). Metabolic pathways in immune cell activation and quiescence. Immunity *38*, 633–643. https://doi.org/10.1016/j.immuni.2013.04.005.

14. O'Neill, L.A.J., Kishton, R.J., and Rathmell, J. (2016). A guide to immunometabolism for immunologists. Nat. Rev. Immunol. *16*, 553–565. https://doi.org/10.1038/nri.2016.70.

15. Karmaus, P.W.F., Chen, X., Lim, S.A., Herrada, A.A., Nguyen, T.L.M., Xu, B., Dhungana, Y., Rankin, S., Chen, W., Rosencrance, C., et al. (2019). Metabolic heterogeneity underlies reciprocal fates of T(H)17 cell stemness and plasticity. Nature *565*, 101–105. https://doi.org/10.1038/s41586-018-0806-7.

16. Gerriets, V.A., Kishton, R.J., Nichols, A.G., Macintyre, A.N., Inoue, M., Ilkayeva, O., Winter, P.S., Liu, X., Priyadharshini, B., Slawinska, M.E., et al. (2015). Metabolic programming and PDHK1 control CD4+ T cell subsets and inflammation. J. Clin. Invest. *125*, 194–207. https://doi.org/10.1172/jci76012.

17. Shi, L.Z., Wang, R., Huang, G., Vogel, P., Neale, G., Green, D.R., and Chi, H. (2011). HIF1alpha-dependent glycolytic pathway orchestrates a metabolic checkpoint for the differentiation of TH17 and Treg cells. J. Exp. Med. *208*, 1367–1376. https://doi.org/10.1084/jem.20110278.

18. Delgoffe, G.M., Kole, T.P., Zheng, Y., Zarek, P.E., Matthews, K.L., Xiao, B., Worley, P.F., Kozma, S.C., and Powell, J.D. (2009). The mTOR kinase differentially regulates effector and regulatory T cell lineage commitment. Immunity *30*, 832–844. https://doi.org/10.1016/j.immuni.2009.04.014.

19. Delgoffe, G.M., Pollizzi, K.N., Waickman, A.T., Heikamp, E., Meyers, D.J., Horton, M.R., Xiao, B., Worley, P.F., and Powell, J.D. (2011). The kinase mTOR regulates the differentiation of helper T cells through the selective activation of signaling by mTORC1 and mTORC2. Nat. Immunol. *12*, 295–303. https://doi.org/10.1038/ni.2005.

20. Shin, B., Benavides, G.A., Geng, J., Koralov, S.B., Hu, H., Darley-Usmar, V.M., and Harrington, L.E. (2020). Mitochondrial oxidative phosphorylation regulates the fate decision between pathogenic Th17 and regulatory T cells. Cell Rep. *30*, 1898–1909.e4. https://doi.org/10.1016/j.celrep.2020.01.022.

21. Palsson-McDermott, E.M., Curtis, A.M., Goel, G., Lauterbach, M.A.R., Sheedy, F.J., Gleeson, L.E., van den Bosch, M.W.M., Quinn, S.R., Domingo-Fernandez, R., Johnston, D.G.W., et al. (2015). Pyruvate kinase M2 regulates Hif-1α activity and IL-1β induction and is a critical determinant of the warburg effect in LPS-activated macrophages. Cell Metabol. *21*, 65–80. https://doi.org/10.1016/j.cmet.2014.12.005.

22. Luo, W., Hu, H., Chang, R., Zhong, J., Knabel, M., O'Meally, R., Cole, R.N., Pandey, A., and Semenza, G.L. (2011). Pyruvate kinase M2 is a PHD3-stimulated coactivator for hypoxia-inducible factor 1. Cell *145*, 732–744. https://doi.org/10.1016/j.cell.2011.03.054.

23. Damasceno, L.E.A., Prado, D.S., Veras, F.P., Fonseca, M.M., Toller-Kawahisa, J.E., Rosa, M.H., Públio, G.A., Martins, T.V., Ramalho, F.S., Waisman, A., et al. (2020). PKM2 promotes Th17 cell differentiation and autoimmune inflammation by fine-tuning STAT3 activation. J. Exp. Med. *217*, e20190613. https://doi.org/10.1084/jem.20190613.

24. Moreno-Fernandez, M.E., Giles, D.A., Oates, J.R., Chan, C.C., Damen, M.S.M.A., Doll, J.R., Stankiewicz, T.E., Chen, X., Chetal, K., Karns, R., et al. (2021). PKM2-dependent metabolic skewing of hepatic Th17 cells regulates pathogenesis of non-alcoholic fatty liver disease. Cell Metabol. *33*, 1187–1204.e9. https://doi.org/10.1016/j.cmet.2021.04.018.

25. Angiari, S., Runtsch, M.C., Sutton, C.E., Palsson-McDermott, E.M., Kelly, B., Rana, N., Kane, H., Papadopoulou, G., Pearce, E.L., Mills, K.H.G., and O'Neill, L.A.J. (2020). Pharmacological activation of pyruvate kinase M2 inhibits CD4(+) T cell pathogenicity and suppresses autoimmunity. Cell Metabol. *31*, 391–405.e8. https://doi.org/10.1016/j.cmet.2019.10.015.

26. Ivanov, I.I., Atarashi, K., Manel, N., Brodie, E.L., Shima, T., Karaoz, U., Wei, D., Goldfarb, K.C., Santee, C.A., Lynch, S.V., et al. (2009). Induction of intestinal Th17 cells by segmented filamentous bacteria. Cell *139*, 485–498. https://doi.org/10.1016/j.cell.2009.09.033.

27. Torchinsky, M.B., Garaude, J., Martin, A.P., and Blander, J.M. (2009). Innate immune recognition of infected apoptotic cells directs T(H)17 cell differentiation. Nature *458*, 78–82. https://doi.org/10.1038/nature07781.

28. Hernández-Santos, N., and Gaffen, S.L. (2012). Th17 cells in immunity to Candida albicans. Cell Host Microbe *11*, 425–435. https://doi.org/10.1016/j.chom.2012.04.008.

29. Kleinewietfeld, M., Manzel, A., Titze, J., Kvakan, H., Yosef, N., Linker, R.A., Muller, D.N., and Hafler, D.A. (2013). Sodium chloride drives autoimmune disease by the induction of pathogenic TH17 cells. Nature *496*, 518–522. https://doi.org/10.1038/nature11868.

30. Wu, C., Yosef, N., Thalhamer, T., Zhu, C., Xiao, S., Kishi, Y., Regev, A., and Kuchroo, V.K. (2013). Induction of pathogenic TH17 cells by inducible salt-sensing kinase SGK1. Nature *496*, 513–517. https://doi.org/10.1038/nature11984.

31. Zhang, D., Jin, W., Wu, R., Li, J., Park, S.A., Tu, E., Zanvit, P., Xu, J., Liu, O., Cain, A., and Chen, W. (2019). High glucose intake exacerbates autoimmunity through reactive-oxygen-species-mediated TGF-β cytokine activation. Immunity *51*, 671–681.e5. https://doi.org/10.1016/j.immuni.2019.08.001.

32. Esplugues, E., Huber, S., Gagliani, N., Hauser, A.E., Town, T., Wan, Y.Y., O'Connor, W., Jr., Rongvaux, A., Van Rooijen, N., Haberman, A.M., et al. (2011). Control of TH17 cells occurs in the small intestine. Nature *475*, 514–518. https://doi.org/10.1038/nature10228.

33. Chen, L., Sun, M., Wu, W., Yang, W., Huang, X., Xiao, Y., Ma, C., Xu, L., Yao, S., Liu, Z., and Cong, Y. (2019). Microbiota metabolite butyrate differentially regulates Th1 and Th17 cells' differentiation and function in induction of colitis. Inflamm. Bowel Dis. *25*, 1450–1461. https://doi.org/10.1093/ibd/izz046.

34. Furusawa, Y., Obata, Y., Fukuda, S., Endo, T.A., Nakato, G., Takahashi, D., Nakanishi, Y., Uetake, C., Kato, K., Kato, T., et al. (2013). Commensal microbe-derived butyrate induces the differentiation of colonic regulatory T cells. Nature *504*, 446–450. https://doi.org/10.1038/nature12721.

35. El-Behi, M., Ciric, B., Dai, H., Yan, Y., Cullimore, M., Safavi, F., Zhang, G.X., Dittel, B.N., and Rostami, A. (2011). The encephalitogenicity of T(H)17 cells is dependent on IL-1- and IL-23-induced production of the cytokine GM-CSF. Nat. Immunol. *12*, 568–575. https://doi.org/10.1038/ni.2031.

36. Lee, Y., Awasthi, A., Yosef, N., Quintana, F.J., Xiao, S., Peters, A., Wu, C., Kleinewietfeld, M., Kunder, S., Hafler, D.A., et al. (2012). Induction and molecular signature of pathogenic TH17 cells. Nat. Immunol. *13*, 991–999. https://doi.org/10.1038/ni.2416.

37. Lloyd-Price, J., Arze, C., Ananthakrishnan, A.N., Schirmer, M., Avila-Pacheco, J., Poon, T.W., Andrews, E., Ajami, N.J., Bonham, K.S., Brislawn, C.J., et al. (2019). Multi-omics of the gut microbial ecosystem in inflammatory bowel diseases. Nature *569*, 655–662. https://doi.org/10.1038/s41586-019-1237-9.

38. Prakasam, G., Iqbal, M.A., Bamezai, R.N.K., and Mazurek, S. (2018). Post-translational modifications of pyruvate kinase M2: tweaks that benefit cancer. Front. Oncol. *8*, 22. https://doi.org/10.3389/fonc.2018.00022.

39. Manel, N., Unutmaz, D., and Littman, D.R. (2008). The differentiation of human T(H)-17 cells requires transforming growth factor-beta and induction of the nuclear receptor RORgammat. Nat. Immunol. *9*, 641–649. https://doi.org/10.1038/ni.1610.

40. Manzel, A., Muller, D.N., Hafler, D.A., Erdman, S.E., Linker, R.A., and Kleinewietfeld, M. (2014). Role of "Western diet" in inflammatory autoimmune diseases. Curr. Allergy Asthma Rep. *14*, 404. https://doi.org/10.1007/s11882-013-0404-6.

41. Endo, Y., Asou, H.K., Matsugae, N., Hirahara, K., Shinoda, K., Tumes, D.J., Tokuyama, H., Yokote, K., and Nakayama, T. (2015). Obesity drives Th17 cell differentiation by inducing the lipid metabolic kinase, ACC1. Cell Rep. *12*, 1042–1055. https://doi.org/10.1016/j.celrep.2015.07.014.

42. Bettelli, E., Carrier, Y., Gao, W., Korn, T., Strom, T.B., Oukka, M., Weiner, H.L., and Kuchroo, V.K. (2006). Reciprocal developmental pathways for the generation of pathogenic effector TH17 and regulatory T cells. Nature *441*, 235–238. https://doi.org/10.1038/nature04753.

43. Mangan, P.R., Harrington, L.E., O'Quinn, D.B., Helms, W.S., Bullard, D.C., Elson, C.O., Hatton, R.D., Wahl, S.M., Schoeb, T.R., and Weaver, C.T. (2006). Transforming growth factor-beta induces development of the T(H)17 lineage. Nature *441*, 231–234. https://doi.org/10.1038/nature04754.

44. Langley, R.G., Elewski, B.E., Lebwohl, M., Reich, K., Griffiths, C.E.M., Papp, K., Puig, L., Nakagawa, H., Spelman, L., Sigurgeirsson, B., et al. (2014). Secukinumab in plaque psoriasis–results of two phase 3 trials. N. Engl. J. Med. *371*, 326–338. https://doi.org/10.1056/NEJMoa1314258.

45. Hueber, W., Sands, B.E., Lewitzky, S., Vandemeulebroecke, M., Reinisch, W., Higgins, P.D.R., Wehkamp, J., Feagan, B.G., Yao, M.D., Karczewski, M., et al. (2012). Secukinumab, a human anti-IL-17A monoclonal antibody, for moderate to severe Crohn's disease: unexpected results of a randomised, double-blind placebo-controlled trial. Gut *61*, 1693–1700. https://doi.org/10.1136/gutjnl-2011-301668.

46. Taams, L.S. (2020). Interleukin-17 in rheumatoid arthritis: trials and tribulations. J. Exp. Med. *217*, e20192048. https://doi.org/10.1084/jem.20192048.

47. Patel, D.D., and Kuchroo, V.K. (2015). Th17 cell pathway in human immunity: lessons from genetics and therapeutic interventions. Immunity *43*, 1040–1051. https://doi.org/10.1016/j.immuni.2015.12.003.

48. Peng, M., Yin, N., Chhangawala, S., Xu, K., Leslie, C.S., and Li, M.O. (2016). Aerobic glycolysis promotes T helper 1 cell differentiation through an epigenetic mechanism. Science *354*, 481–484. https://doi.org/10.1126/science.aaf6284.

49. Macintyre, A.N., Gerriets, V.A., Nichols, A.G., Michalek, R.D., Rudolph, M.C., Deoliveira, D., Anderson, S.M., Abel, E.D., Chen, B.J., Hale, L.P., and Rathmell, J.C. (2014). The glucose transporter Glut1 is selectively essential for CD4 T cell activation and effector function. Cell Metabol. *20*, 61–72. https://doi.org/10.1016/j.cmet.2014.05.004.

50. Raez, L.E., Papadopoulos, K., Ricart, A.D., Chiorean, E.G., Dipaola, R.S., Stein, M.N., Rocha Lima, C.M., Schlesselman, J.J., Tolba, K., Langmuir, V.K., et al. (2013). A phase I dose-escalation trial of 2-deoxy-D-glucose alone or combined with docetaxel in patients with advanced solid tumors. Cancer Chemother. Pharmacol. *71*, 523–530. https://doi.org/10.1007/s00280-012-2045-1.

51. Li, H.B., Tong, J., Zhu, S., Batista, P.J., Duffy, E.E., Zhao, J., Bailis, W., Cao, G., Kroehling, L., Chen, Y., et al. (2017). m(6)A mRNA methylation controls T cell homeostasis by targeting the IL-7/STAT5/SOCS pathways. Nature *548*, 338–342. https://doi.org/10.1038/nature23450.

52. Zhu, S., Pan, W., Song, X., Liu, Y., Shao, X., Tang, Y., Liang, D., He, D., Wang, H., Liu, W., et al. (2012). The microRNA miR-23b suppresses IL-17-associated autoimmune inflammation by targeting TAB2, TAB3 and IKK-α. Nat. Med. *18*, 1077–1086. https://doi.org/10.1038/nm.2815.

53. Chou, W.C., Guo, Z., Guo, H., Chen, L., Zhang, G., Liang, K., Xie, L., Tan, X., Gibson, S.A., Rampanelli, E., et al. (2021). AIM2 in regulatory T cells restrains autoimmune diseases. Nature *591*, 300–305. https://doi.org/10.1038/s41586-021-03231-w.

54. Dieleman, L.A., Palmen, M.J., Akol, H., Bloemena, E., Peña, A.S., Meuwissen, S.G., and Van Rees, E.P. (1998). Chronic experimental colitis induced by dextran sulphate sodium (DSS) is characterized by Th1 and Th2 cytokines. Clin. Exp. Immunol. *114*, 385–391. https://doi.org/10.1046/j.1365-2249.1998.00728.x.

STAR★METHODS

KEY RESOURCES TABLE

REAGENT or RESOURCE	SOURCE	IDENTIFIER
Antibodies		
Anti-mouse CD4 APC (clone GK1.5)	Biolegend	Cat# 100412; RRID:AB_312697
Anti-mouse CD45.2 APC-Cy7 (clone 104)	Biolegend	Cat# 109824; RRID:AB_830789
Anti-mouse CD69 PerCP-Cy5.5 (clone H1.2F3)	Biolegend	Cat# 104522; RRID:AB_2260065
Anti-mouse CD4 PerCP-Cy5.5 (clone GK1.5)	Biolegend	Cat# 100434; RRID:AB_893324
Anti-mouse CD4 FITC (clone GK1.5)	Biolegend	Cat# 100406; RRID:AB_312691
Anti-mouse CD25 APC (clone PC61)	Biolegend	Cat# 102012; RRID:AB_312861
Anti-mouse CD45RB PE (clone C363-16A)	Biolegend	Cat# 103308; RRID:AB_313015
Anti-mouse Ki-67 PE (clone 16A8)	Biolegend	Cat# 652404; RRID:AB_2561525
Anti-mouse IL-17A PE (clone TC11-18H10.1)	Biolegend	Cat# 506904; RRID:AB_315464
Anti-mouse IFN-γ PE-Cy7 (clone XMG1.2)	Biolegend	Cat# 505826; RRID:AB_2295770
Anti-mouse GM-CSF APC (MP1-22E9)	Biolegend	Cat# 505414; RRID:AB_2721461
Anti-mouse IL-4 PE (clone 11B11)	Biolegend	Cat# 504104; RRID:AB_315318
Anti-mouse IL-13 PE (clone W17010B)	Biolegend	Cat# 159403; RRID:AB_2832569
Anti-mouse FoxP3 PE (clone MF-14)	Biolegend	Cat# 126404; RRID:AB_1089117
Anti-human CD4 Alexa Fluor® 647 (clone OKT4)	Biolegend	Cat# 317422; RRID:AB_571941
Anti-human IL-17A BV421 (clone BL168)	Biolegend	Cat# 512321; RRID:AB_10899566
Ultra-LEAF™ Purified anti-mouse CD3 (clone 172)	Biolegend	Cat# 100253; RRID:AB_2810314
Ultra-LEAF™ Purified anti-mouse CD28 (clone 37.51)	Biolegend	Cat# 102121; RRID:AB_2810330
Ultra-LEAF™ Purified anti-mouse IL-4 (clone 11B11)	Biolegend	Cat# 504135; RRID:AB_2750404
Ultra-LEAF™ Purified anti-mouse IFN-γ (clone XMG1.2)	Biolegend	Cat# 505847; RRID:AB_2616675
Ultra-LEAF™ Purified anti-human CD3 (clone UCHT1)	Biolegend	Cat# 300438; RRID:AB_11146991
Ultra-LEAF™ Purified anti-human CD28 (clone CD28.2)	Biolegend	Cat# 302934; RRID:AB_11148949
Anti-Phospho-STAT3 (Tyr 705)	Cell Signal Technology	Cat# 9145; RRID:AB_2491009
Anti-Phospho-PKM2 (Tyr 105)	Cell Signal Technology	Cat# 3827; RRID:AB_1950369
Anti-PKM2	Cell Signal Technology	Cat# 4053; RRID:AB_1904096
Anti-β-Actin	Sigma	Cat# A5316; RRID:AB_476743
Anti-Lamin B1	Proteintech	Cat# 12987-1-AP; RRID:AB_2136290
Anti-GAPDH	Proteintech	Cat# 10494-1-AP; RRID:AB_2263076
Goat anti-mouse IgG-HRP	Beyotime	Cat# A0216; RRID:AB_2860575
Goat anti-rabbit IgG-HRP	Beyotime	Cat# A0208; RRID:AB_2892644
Biological samples		
Fetal Bovine Serum	ThermoFisher	Cat# 10091148
Chemicals, peptides, and recombinant proteins		
Recombinant human IL-2	Biolegend	Cat# 589102
Recombinant human TGFβ1	Biolegend	Cat# 580704

(*Continued on next page*)

Continued

REAGENT or RESOURCE	SOURCE	IDENTIFIER
Recombinant mouse IL-4	Biolegend	Cat# 574304
Recombinant mouse IL-6	Biolegend	Cat# 575704
Recombinant mouse IL-12	Biolegend	Cat# 577002
Recombinant mouse IL-23	Biolegend	Cat# 589002
Recombinant human IL-6	Biolegend	Cat# 570802
Recombinant human IL-1β	Biolegend	Cat# 579402
7-AAD Viability Staining Solution	Biolegend	Cat# 420403
DAPI	Biolegend	Cat# 422801
Annexin V Alexa Fluor® 647	Biolegend	Cat# 640943
Incomplete Freund's adjuvant	Difco Laboratories	Cat# BD 263910
Mycobacterium tuberculosis H37RA	Difco Laboratories	Cat# BD 231141
Pertussis toxin	List Biological	Cat# 180
Myelin oligodendrocyte glycoprotein (MOG) peptide 35–55	QYAOBIO	Cat# 163913-87-9
Disuccinimidyl suberate (DSS)	ThermoFisher	Cat# 21655
RPMI 1640 medium	ThermoFisher	Cat# 22400089
SYBR qPCR Master MIX	Vazyme	Q311-02
HiScript® III RT SuperMix for qPCR	Vazyme	R323-01
TRNzol Universal Reagent	TIANGEN	Cat# 4992730
Percoll	Sigma	Cat# GE17-0891-01
DNase I	Sigma	Cat# 11284932001
Collagenase Type II	Sigma	Cat# C6885
Penicillin-streptomycin	Gibco	Cat# 10378016
H2DCFDA	ThermoFisher	Cat# D399
MitoTracker™ Deep Red FM Dye	ThermoFisher	Cat# M46753
PZ-2891	MCE	Cat# HY-124634
TEPP-46	MCE	Cat# HY-18657
Coenzyme A Hydrate	Sigma	C4282
D-Pantothenic acid hemicalcium salt	Sigma	P5155
Coenzyme A-Agarose	Sigma	C7013
Immobilon Western Chemiluminescent HRP Substrate	Millipore	WBKLS0500
Biotin-labeled Goat Anti-mouse IgG(H + L)	Beyutime	A0288
Biotin-labeled Goat Anti-rabbit IgG(H + L)	Beyutime	A0277
Critical commercial assays		
MojoSort™ Mouse naive CD4 T cell Isolation Kit	Biolegend	Cat# 480040
MojoSort™ Human CD4 Naive T cell Isolation Kit	Biolegend	Cat# 480041
Fixation/Permeabilization Solution Kit	BD Bioscience	Cat# 554714
Cell Stimulation Cocktail (plus protein transport inhibitors)	eBioscience	Cat# 00-4975-93
eBioscience™ Foxp3/Transcription Factor Staining Buffer Set	eBioscience	Cat# 00-5523-00
Human IL-17A Precoated ELISA Kit	DAKEWE	Cat# 1111702
Mouse IL-17 ELISA Kit	absin	Cat# abs520009
Nuclear and Cytoplasmic Protein Extraction Kit	Beyotime	Cat# P0028
Seahorse Cell Mito Stress Test kit	Agilent	Cat# 103015-100
Seahorse Cell Glycolysis Stress Test kit	Agilent	Cat# 103017-100

(*Continued on next page*)

Continued

REAGENT or RESOURCE	SOURCE	IDENTIFIER
VB5 ELISA KIT	J&L BIOLOGY	Cat# JL46633
CellTrace Violet cell proliferation kit	ThermoFisher	Cat# C34557
Coenzyme A Assay Kit	Abcam	Ab102504
Zombie Aqua™ Fixable Viability Kit	Biolegend	Cat# 423102
Deposited data		
RNA sequencing data	This paper	BioProject: PRJNA879881
Experimental models: Organisms/strains		
Mouse: C57BL/6JGpt	GemPharmatech	Strain no. N000013
Mouse: B6/JGpt-Rag1em1Cd/Gpt	GemPharmatech	Strain no. T004753
Oligonucleotides		
qPCR primers for various genes	This paper	Table S3
Software and algorithms		
FlowJo software version 10.6.2	FlowJo, LLC	https://www.flowjo.com/
Prism version 9	Graphpad	https://www.graphpad.com/
Image-Pro Plus 6.0	Image-Pro Plus	https://www.mediacy.com/company/about
Image Lab 5.2.1	Image Lab	https://www.bio-rad.com/en-hk/product/image-lab-software?ID=KRE6P5E8Z
SnapGene 3.2.1	SnapGene	https://www.snapgene.com/
Bio-Rad CFX Manager 3.1	Bio-Rad CFX Manager	https://www.bio-rad.com/en-hk/sku/1845000-cfx-manager-software?ID=1845000

RESOURCE AVAILABILITY

Lead contact

Further information and requests for resources and reagents should be directed to and will be fulfilled by the lead contact, Shu Zhu (zhushu@ustc.edu.cn).

Materials availability

This study did not generate new, unique reagents.

Data and code availability

- All data necessary to understand and evaluate the conclusions of this paper are provided in the manuscript and supplementary materials. The raw bulk RNA-seq data in this study were deposited in the NCBI BioProject repository under accession number PRJNA879881. Original western blot images have been deposited at Mendeley Data at https://doi.org/10.17632/ptftdjfjyv.1.
- This paper does not report original code.
- Any additional information required to reanalyze the data reported in this paper is available from the lead contact upon request.

EXPERIMENTAL MODEL AND SUBJECT DETAILS

Human subjects

All human samples used in the present study were obtained with the approval of the first affiliated hospital of the USTC (Anhui Provincial Hospital) (2021KY02). Blood sample from UC patients (n = 31) and health (n = 21) were collected from the First Affiliated Hospital of University of Science and Technology of China (Hefei, China). Blood samples from MS patients (n = 8) were collected from Nanjing Drum Tower Hospital. The patients were diagnosed on the basis of standard clinical, endoscopic, and histological criteria for IBD. The demographic and clinical characteristics of the studied populations are shown in the Table S2.

Mice

IL-17A–IRES–GFP reporter mice were provided by Dr. Richard A. Flavell of Yale University School of Medicine. C57BL/6 mice were purchased from GemPharmatech. In all experiments, 6–8-week-old, age- and sex-matched mice in C57BL/6 background were used. Mice were maintained under specific pathogen free (SPF) conditions under a strict 12-h light cycle (lights on at 08:00 and off at 20:00).

All animal studies were performed according to approved protocols by the Ethics Committee of the University of Science and Technology of China (USTCACUC212101033).

Cell culture

Primary mouse $CD4^+$ T cells from spleens and lymph nodes were isolated by mouse naive $CD4^+$ T cell Isolation Kit (BioLegend). Isolated mouse naive $CD4^+$ T cells were activated in 96 well-plate pre-coated with 2 μg/mL anti-mouse CD3 and 1 μg/mL anti-mouse CD28 mAb. Human primary $CD4^+$ T cells from peripheral blood mononuclear cell (PBMC) of healthy donors were isolated by human naive $CD4^+$ T cell Isolation Kit (BioLegend). Isolated human naive CD4 T cells were activated in 96 well-plate pre-coated with 2 μg/mL anti-human CD3 and 1 μg/mL anti-human CD28 mAb. All cells were cultured at 37°C in 5% CO_2-containing humidified incubators.

METHOD DETAILS

T cell–transfer colitis

We performed the experiment as previously described.[51] Briefly, $CD4^+CD25^-CD45RB^{high}$ T cells were isolated from spleens and peripheral lymph nodes of C57BL/6 mice using a FACSAria (FACSAria III, BD) and injected into *Rag1*$^{-/-}$ mice (5 x 10^5 cells per mouse) to induce colitis by intraperitoneal injection. Mice were fed a normal diet or VB5-deficient diet or water containing 50mg/kg/day VB5 (started two days before T cell transfer). The mice were monitored the development of colitis every week. Colon, spleen, and mLN tissues were harvested at the end of the experiments for histopathological and immunological analysis.

EAE induction

The EAE model was established as previously described.[52] Briefly, male mice (aged of 8 weeks) were immunized (subcutaneous injection on both dorsal sides) with $MOG_{35–55}$ peptides (300 μg/mouse) emulsified in complete Freund's adjuvant, containing 5 mg/mL heat-killed *Mycobacterium tuberculosis* H37Ra, and 200 ng pertussis toxin (PTX, dissolved in 0.1 mL of PBS) was injected intravenously. Mice were treated with a normal diet or a VB5-deficient diet or water containing 50mg/kg/day VB5 (started 2 weeks before immunization). Mice were then observed daily for disease development.

For passive transfer induced EAE, naive CD4 T cells were differentiated under Th17-skewing conditions for 96 h, then IL-17A-GFP positive cells were sorted by using a FACSAria (FACSAria III, BD) and injected intravenously into *Rag1*$^{-/-}$ mice (1 x 10^6 cells per mouse). Two days after T cell transfer, recipient mice were immunized with $MOG_{35–55}$ peptides (300 μg/mouse) emulsified in complete Freund's adjuvant, containing 5 mg/mL heat-killed *Mycobacterium tuberculosis* H37Ra, and 200 ng pertussis toxin (PTX, dissolved in 0.1 mL of PBS) was injected intravenously. Mice were then observed daily for disease development.

EAE clinical scores were assessed as follows: 0, no clinical signs; 1, limp tail; 2, paraparesis (weakness, incomplete paralysis of one or two hind limbs); 3, paraplegia (complete paralysis of two hind limbs); 4, paraplegia with forelimb weakness or paralysis; 5, moribund or death.

T cell activation, differentiation, and proliferation *in vitro*

2 x 10^5 naive $CD4^+$ T cells were isolated and activated in 96 well-plate pre-coated with 2 μg/mL anti-CD3 and 1 μg/mL anti-CD28 mAb. For Th17 cell differentiation, a cocktail of 25 ng/mL mouse IL-6 (Biolegend), 20 ng/mL mouse IL-23 (Biolegend), 2 ng/mL human TGFβ1 (Biolegend), 5 μg/mL anti-mouse IFN-γ and 5 μg/mL anti-mouse IL-4 was added to the culture. For Th1 cell differentiation, a cocktail of 50 U/mL human IL-2 (Biolegend), 20 ng/mL mouse IL-12 (Biolegend) and 5 μg/mL anti-mouse IL-4 was added to the culture. For Th2 cell differentiation, a cocktail of 50 U/mL human IL-2 (Biolegend), 20 ng/mL mouse IL-4 (Biolegend) and 5 μg/mL anti-mouse IFN-γ was added to the culture. For Treg cell differentiation, a cocktail of 500 U/mL human IL-2 (Biolegend), 5 ng/mL human TGFβ1 (Biolegend), 5 μg/mL anti-mouse IL-4 and 5 μg/mL anti-mouse IFN-γ was added to the culture. VB5, CoA and PZ-2891 were added when needed as indicated in the figure legends. To assess proliferation, isolated $CD4^+$ T Cells were labeled with 2.5 μM CellTrace Violet (CTV) for 15 min at 37°C. Labeled T cells were washed with 1x PBS containing 0.5% FBS and activated under condition as indicated in the figure legends. The T cell proliferation was assessed at 96 h post activation based on CTV dilution by flow cytometry.

For human Th17 cell differentiation, human naive $CD4^+$ T cells were cultured for 7 days in 96-well flat bottom plates with pre-coated 2 μg/mL anti-human CD3, and 1 μg/mL soluble anti-human CD28, a cocktail of 50 ng/mL human IL-6 (Biolegend), 2 ng/mL human TGFβ1 (Biolegend), 50 ng/mL human IL-1β (Biolegend) were added.

Isolation of lymphocytes from the lamina propria, spinal cord, and lymph nodes

For isolating mononuclear cells from the lamina propria, the intestine (small and/or large) was removed immediately after euthanasia, and was carefully stripped of mesenteric fat and Peyer's patches/cecal patch. The intestine was turned inside out and cut into 1 cm sections then transferred into RPMI with 2 mM EDTA and shaken for 20 min at 37°C for 3 times. The supernatants were then discarded. Tissue sections were collected and washed with RPMI (EDTA-free) for another 5 min. The intestinal sections were transferred into digestion buffer (RPMI with 0.5 mg/mL collagenases II, Sigma C6885; 0.5 mg/mL DNase I, Sigma; and 5% FBS) and shaken for 30 min at 37°C. The supernatants were collected through a 70 μm cell strainer to obtain single cell suspensions as lamina propria lymphocytes (LPL). Mononuclear cells from the SC, brain, spleen, mesenteric lymph nodes (for the colitis model), and draining lymph

nodes (inguinal lymph nodes for the EAE model) were mechanically dissected and minced in RPMI containing 10% FBS through 70 μm strainer. Cells were collected for further analysis.

Flow cytometry

For surface staining, single-cell suspensions were incubated at 4°C with conjugated antibodies in PBS containing 0.5% FBS and 2 mM EDTA for 20 min. For intracellular cytokine staining, cells were first incubated for 4 h in RPMI with 10% FBS, Cell Stimulation Cocktail (500X). Then $1x10^6$ cells were fixed/permeabilized for 20 min at 4°C with Fixation/Permeabilization Solution Kit (BD Bioscience) and stained with fluorescently-conjugated antibodies per manufacture's protocols. After wash, cells were analyzed using CytoFlex s (Beckman Coulter). FACS data were analyzed using FlowJo v.10. The staining antibodies for flow cytometry (all used at 1:200 unless otherwise indicated) were purchased from Biolegend.

Real-time PCR

For cells and tissues, total RNA was extracted with TRIzol reagent (TIANGEN) according to the manufacturer's instructions. One microgram of total RNA was reverse-transcribed to generate cDNA with Superscript (Vazyme). Quantitative real-time PCR was performed using SYBR qPCR Master MIX (Vazyme) on a Real-Time PCR System (Bio-Rad). The target genes were normalized to the housekeeping gene (*Hprt*). Fold changes were presented as a result of $2^{-\Delta\Delta Ct}$. Relative gene expression was presented as a result of $2^{-\Delta Ct}$. Primer sequences were based on Primer-Bank (http://pga.mgh.harvard.edu/primerbank) and blasted to confirm target genes using Primer-Blast (http://www.ncbi.nlm.nih.gov/tools/primer-blast).

H&E staining and LFB staining

The tissues were fixed in 4% PFA and embedded in paraffin. Sections were stained with hematoxylin, eosin or Luxol fast blue. Morphological changes in stained sections were examined under a light microscope (BX53, Olympus) for morphology. The number of inflammatory foci and total demyelination were measured using methods described previously.[53] In brief, the numbers of inflammatory foci that contained at least 20 cells were counted within each H&E-stained section in a blinded fashion. Estimates were made of the number of foci, when foci coalesced. Areas of demyelination were assessed in LFB- eosin–stained sections. Image-Pro Plus software was used to manually trace the total cross-sectional area and the demyelinated area of each section. Total demyelination was expressed as a percentage of the total spinal cord area.[53] The distal colons of colitis mice were fixed in 4% PFA, dehydrated in a 10%–20%-30% sucrose gradient buffer. For each distal colon, four transversal sections cut from different areas were stained with hematoxylin & eosin (H&E). The histopathological score for each section was determined by summation of the scores from each category as described.[54] In brief, the histological scores include presence of ulcer (0 = none, 1 = punctate, 2 = minimal, 3 = moderate, 4 = widespread), presence of inflammation (0 = none, 1 = minimal, 2 = mild, 3 = moderate, 4 = severe), extent of inflammation (0 = none, 1 = mucosal, 2 = mucosal + submucosal, 3 = mucosal + submucosal + muscle penetrate, 4 = full thickness involvement). The total histopathological score was the sum of the three sections scores.

Metabolism assays

OCR and ECAR were measured with an XF96 extracellular flux analyzer (Seahorse Bioscience) following protocols recommended by the manufacturer. Briefly, activated T cells were seeded on XF96 microplates (500,000 cells/well) that had been pre-coated with poly-L-Lysine (20 μg/mL). The plates were quickly centrifuged to immobilize cells. Cells were maintained in a non-buffered assay medium (Seahorse Biosciences) in a non-CO_2 incubator for 30 min before the assay. Glycolysis was measured with XF glycolysis stress test kit (Seahorse Biosciences). Initially, cells were incubated in the glycolysis stress test medium without glucose, and ECAR was assessed. Three baseline recordings were made, followed by sequential injection of 10 mM glucose and 1 μM oligomycin that inhibited mitochondrial ATP production and shifted the energy production to glycolysis. The increased ECAR revealed the maximum glycolytic capacity of T cells. The final injection was 50 mM 2-DG, a glucose analog that inhibited glycolysis. The resulted decrease of ECAR confirmed that the ECAR observed in experiments was due to glycolysis. The Mito stress test kit (Seahorse Biosciences) was used to test OCR under different conditions. Three baseline recordings were made, followed by sequential injection of 1 μM oligomycin, 1.5 μM FCCP that uncoupled oxygen consumption from ATP production to obtain maximal OCR, and 1 μM rotenone/antimycin A that inhibited complex I and III. Measurements for each experiment were made in triplicate. Basal respiration, ATP production, spare respiratory capacity (SRC), and coupling efficiency were calculated as follows: Basal respiration = OCR before oligomycin treatment minus OCR after rotenone/antimycin A (non-mitochondrial respiration); Maximal respiration = the maximal OCR after FCCP treatment minus OCR after rotenone/antimycin A (non-mitochondrial respiration); The SRC was calculated as the maximal OCR after FCCP treatment minus the OCR before oligomycin treatment. Glycolysis = maximum rate measurement before oligomycin injection minus last rate measurement before glucose injection; Glycolytic capacity = maximum rate measurement after oligomycin injection minus last rate measurement before glucose injection.

LC/MS analysis

T cell non-targeted energy metabolomics were performed by Shanghai Applied Protein Technology (Shanghai, China) using LC-MS/MS. In brief, $1x10^8$ Th17 cells, 200 μL ultrapure water, and 800 μL methanol/acetonitrile (1:1, v/v) were first added into an EP tube. Then, the sample was homogenized with an MP homogenizer and ultrasonic instrument, incubated at −20°C for 60 min, and

centrifuged at 14,000 rpm at 4°C for 15 min. The supernatant was collected and subjected to mass spectrometry analysis with a 5500 QTRAP mass spectrometer (AB-SCIEX). Multiquanta software was used to extract the peak area and retention time, which were normalized to the standard energy metabolism substance for metabolite identification. For clustering analysis, the quantitative information of the target metabolite set was first normalized to (−1, 1) intervals, and then cluster 3.0 software and Java Tree view software were used to analyze the expression of samples and metabolites, and to generate a hierarchical clustering heatmap.

Immunoprecipitation

CoA agarose immunoprecipitation was performed according to the manufacturer's instructions. Briefly, the splenocytes were lysed in lysis buffer (50 mM Tris-HCl, pH 7.4, 0.5% NP-40, 2 mM EDTA, and 150 mM NaCl, with complete protease inhibitors). The lysates were cleared by centrifugation and then incubated for 2 h with CoA agarose beads (Sigma–Aldrich). After four times washes with lysis buffer, proteins bound to CoA agarose beads were extracted for western blotting or mass spectrum.

Cross-linking reaction and western blotting

Th17 cells were cross-linked with 500 μM disuccinimidyl suberate (Thermo Scientific) for 30 min at 37°C, and then cell lysates were prepared with lysis buffer (50 mM Tris-HCl, pH 7.4, 0.5% NP-40, 2 mM EDTA, and 150 mM NaCl, with complete protease inhibitors). Protein samples were resolved on SDS-PAGE gels and transferred into a polyvinylidene difluoride (PVDF) membrane via wet transfer. The membranes were probed with primary antibodies with specific dilution and secondary HRP-conjugated antibodies at a 1:5000 dilution. Images were analyzed with Image Lab software (Bio-Rad).

Quantification and statistical analysis

Statistical analysis of the results was performed using GraphPad Prism (Version 9, GraphPad software). No statistical method was used to predetermine the sample size. A two-tailed Student's t test was used to compare two groups of samples. $p < 0.05$ (confidence interval of 95%) was considered statistically significant. In the Figures, *, **, *** and **** were used to indicate $p < 0.05$, $p < 0.01$, $p < 0.001$ and $p < 0.0001$, respectively. For all bar graphs, data were expressed as mean ± s.e.m. The sample sizes (biological replicates), specific statistical tests used, and the main effects of our statistical analyzes for each experiment are detailed in each Figure legends.